4.1 Introduction

The main organic synthesis relies heavily on reactions that produce carbon-carbon bonds to create complex, functionalized compounds from widely available substrates. Visible light has recently experienced a surge that has mirrored a breakthrough in organic synthesis because of its powerful ability to form bonds. Developing C-C bond by visible-light-initiated photoredox catalysis via C(sp^3)-H functionalization has recently attracted much attention due to its low cost, environment-friendly, sustainable, and green properties [1-6].

Alkynes serve significant structural roles in an array of organic compounds, bioactive molecules, and natural products [7]. Researchers in synthetic organic laboratories frequently use alkynes as intermediates for a range of target-oriented compounds and directly open the door to functionalized cyclic or acyclic products [8-10].

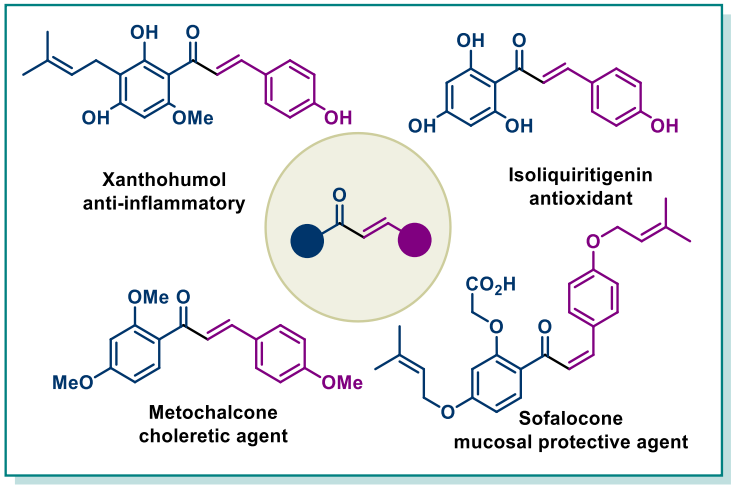

Figure 4.1 Biologically active α, β-unsaturated ketones

Hydroacylation entails introducing an acyl group across the π-bond of an alkyne or alkene to form an enone or a ketone, respectively [11-12]. One could produce α, β-unsaturated

ketones (chalcones) by hydroacylating terminal alkynes, which is a significant, effective, and ecologically friendly way to create C-C bonds from C-H bonds [13-15].

In synthetic organic chemistry, α, β-unsaturated ketones have been widely used as adaptable substances, such as vital substrates for Michael addition, Diels-Alder, Morita-Baylis-Hillman, and epoxidation reactions. α, β-unsaturated ketones containing natural and synthetic chalcones have been the subject of extensive research in medicinal chemistry in the twenty-first century as they have a wide range of biological potential that are fascinating and useful in therapeutic development, such as anti-inflammatory [16,17], antibiotic [18,19], antioxidant [20], anticancer [21], antiplatelet [22], antidiabetic [23], aldose reductase inhibition [24], acetylcholinesterase inhibition [25], immunomodulatory [26], and as non-purine xanthine oxidase inhibitors [27]. Several chalcone-based medications like metachalcone [28], a choleretic drug, are used. Chalcones have reportedly been found to suppress SARS-CoV-2 (COVID-19) [29,30] recently. They are also excellent tools for synthesizing organic compounds, particularly heterocycles (Figure 4.1) [31].

Because of their enormous significance in chemistry and biology, chalcones (α, β-unsaturated ketones) have undergone in-depth study and have been produced using various synthetic techniques [11,32-35]. Although these methods are highly efficient for producing chalcones, most of them are expensive and environment harmful. Moreover, the hydroacylation of alkynes can result in the synthesis of chalcones [14,15,36-40] (Scheme 4.1a-c).

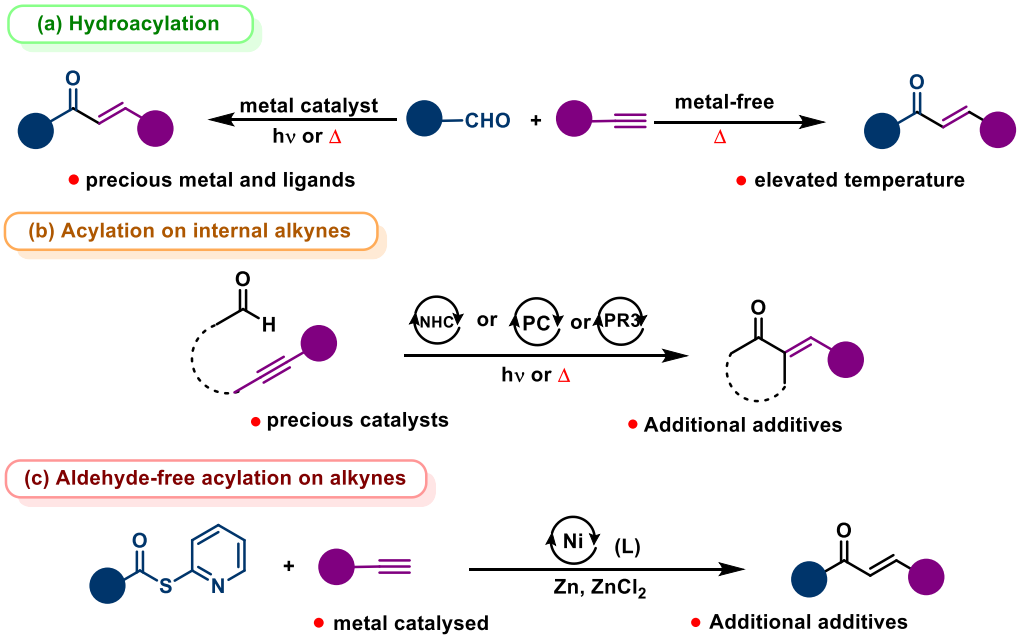

Scheme 4.1 Various Strategies for hydroacylation of alkynes

Aldehydes, α-Oxo Acids, etc., have been used as acyl radical precursors for hydroacylation [41,42]. In this methodology, we have incorporated methyl arenes as an acyl radical precursor via C(sp^3)-H functionalization for the first time. Hence, there has been a rapid increase in interest in using organic dyes as metal-free photocatalysts enabled by photo-energy, which offers excellent prospects for creating ecologically sustainable and effective methods for achieving molecular assembly [4,43- 45].

Enlightened by the advancements in sustainable development and ongoing investigation into photo-induced reactions using organic photocatalysts in our laboratory [46-52] herein, we have developed a green, effective, gentle, and metal-free protocol for the synthesis of chalcones through photocatalytic hydroacylation of terminal alkynes under mild conditions and ambient air as oxidant (Scheme 4.2).

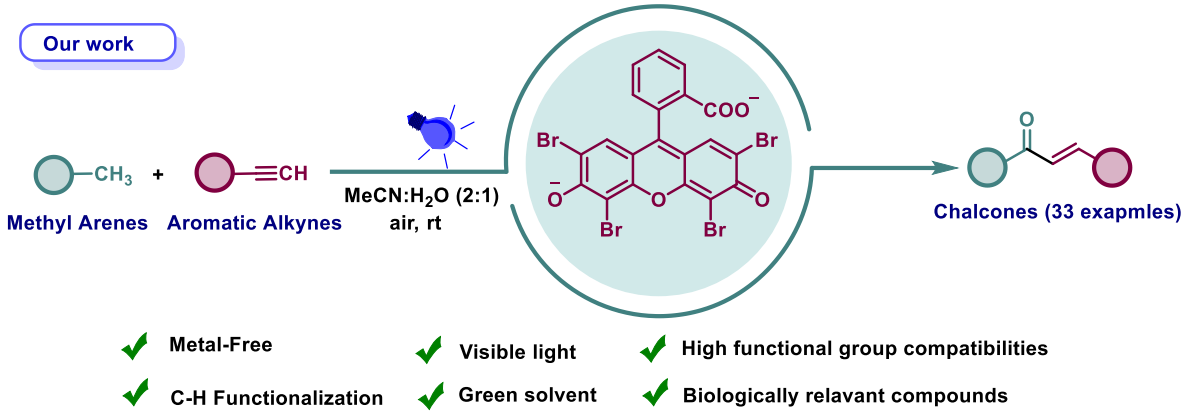

Scheme 4.2 Hydroacylation of alkynes with methyl arenes

4.2 Results and Discussion

To support our hypothesis, we screened the transformation parameters of photocatalyzed C(sp^3)-H activation for the hydroacylation of terminal alkynes (Table 4.1). Initially, the reaction was conducted by taking toluene (**1a**) and phenylacetylene (**2a**) using eosin Y (PC I) as a photocatalyst in ethanol under ambient atmosphere and blue light irradiation, and the target product (**3a**) was produced in 38% yield (Table 4.1 entry 1).

The impact of various photocatalysts was assessed by replacing PC I with metal-free photocatalysts PC II, PC III, and PC IV, leading to a reduced yield of product (Table 4.1 entries 2-4). More screening into different polar and non-polar solvents revealed that MeCN was the ideal reaction medium for the present photocatalytic reaction (Table 4.1 entry 5-14). Water quantity had an effect, which was investigated by taking different ratios of MeCN and water, and the best result (81%) was obtained when MeCN and water were used in a ratio of 2:1 (Table 4.2 entries 1-5). Different eosin Y loading showed that 3 mol% was still the best (Table 4.3 entries 1-4).

Tables 4.1 Optimization Table for Reaction Conditions [a]

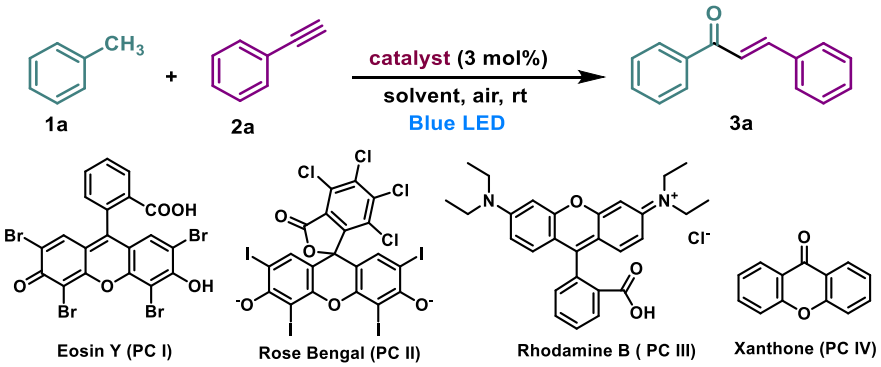

Entry	Catalyst	Solvent	Yield [b] (%)
1	PC I	EtOH	38
2	PC II	EtOH	trace
3	PC III	EtOH	trace
4	PC IV	EtOH	trace
5	PC I	ethanol	27
6	PC I	toluene	15
7	PC I	THF	22
8	PC I	DMSO	trace
9	PC I	DMF	trace
10	PC I	H_2O	44
11	PC I	MeCN	46
12	PC I	DCM	trace
13	PC I	acetone	trace
14	PC I	dioxane	31

[a]Reaction Condition: toluene (0.25 mmol), ethynylbenzene (0.25 mmol), catalyst (3 mol %), solvent (5 mL), Blue LED (18 h) under open air at room temperature. [b]isolated yield

Table 4.2 Screening of ratio of MeCN:Water [a]

Entry	Ratio of MeCN: H_2O	Yield [b] (%)
1	MeCN:H_2O (1:1)	70
2	MeCN:H_2O (1:2)	74
3	MeCN:H_2O (1:3)	77
4	MeCN:H_2O (2:1)	81
5	MeCN:H_2O (3:1)	79

[a]Reaction Condition: toluene (0.25 mmol), ethynylbenzene (0.25 mmol), eosin Y (3 mol %), MeCN:H_2O (5mL), Blue LED (18h) under open air at room temperature. [b]isolated yield

Table 4.3 Screening of amount of photocatalyst and time [a]

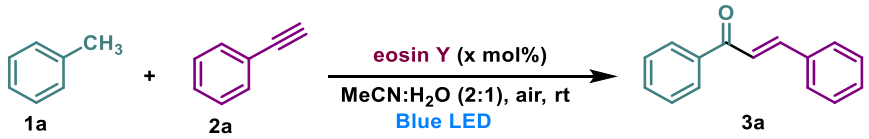

Entry	Eosin Y (mol %)	Time (h)	Yield [b] (%)
1	3	18	81
2	1	18	72
3	2	18	76
4	4	18	79
5	3	14	74
6	3	16	76

7	3	20	78
8	3	22	80

[a]Reaction Condition: toluene (0.25 mmol), ethynylbenzene (0.25 mmol), eosin Y (3 mol %), MeCN:H_2O (2:1) (5 mL), Blue LED under open air at room temperature. [b]isolated yield

The desired product's yield was lowered when the light source was changed (Table 4.4 entries 2-6). In the absence of either the photocatalyst or visible light, the cross-coupling process was terminated, emphasizing the necessity of these parameters (Table 4.4 entry 1). We observed that the target product's yield was unaffected by time fluctuation (Table 4.3 entries 5-8).

Table 4.4 Screening of different color LEDs [a]

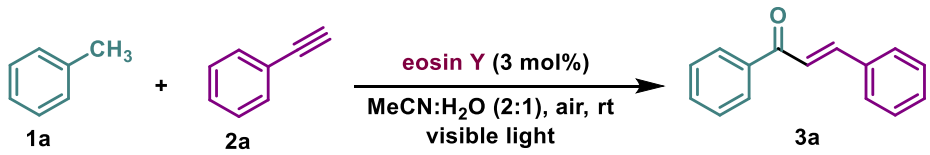

Entry	variations in the reaction conditions	Yield [%]b
1	in dark	nr
2	green LEDs instead of blue LEDs	35
3	purple LEDs instead of blue LEDs	72
4	White LEDs instead of blue LEDs	75
5	20W CFL instead of blue LEDs	70
6	blue LEDs	81

[a]Reaction Condition: toluene (0.25 mmol), ethynylbenzene (0.25 mmol), eosin Y (3 mol %), MeCN:H_2O (2:1) (5 mL), in visible light (18 h) under open air at room temperature. [b]isolated yield

Using the optimized reaction conditions, we examined the generality of the substrate for the hydroacylation with different aromatic alkynes **(2)** and methyl arenes **(1)** in an (*E*)-specific fashion (Table 4.5). First, we investigated the variety of aromatic alkynes, and the findings suggested that the approach has strong functional group compatibility. Alkynes with different electrical and steric characteristics in their aryl groups were well tolerated and produced the desired acylated α, β-unsaturated ketones in good to excellent yields (Table 4.5a).

Halogens and other functional groups like methyl, methoxy, hydroxy, and nitro were well tolerated and afforded the desired product in 81-88% yields **(3a-3c, 3h-3k)**. Additionally, the efficiency of this transition is not significantly affected by the steric restriction of substitutes on the aryl group **(3d-3g)**. Di-substituted benzene rings and 1-ethynyl naphthalene successfully produced the chalcones in 77-89%, and 75% yields **(3l-3n & 3o)**. Aromatic alkynes with thiophene rings generated heteroaromatic chalcones in 67% yields **(3p)**. With cyclohexylacetylene **(3q)** the yield decreased to 49%. Next, we focused our attention on disubstituted alkynes, but no product was formed. (maybe due to steric hindrance provided by the attached group to the incoming acyl radical).

After demonstrating the generality of aromatic alkynes, we next screened the scope of the methyl arenes. The formal hydroacylation proceeded well to produce the appropriate chalcones in high yields when methyl arene substituted at the *o*-, *m*-, *or p*-position were utilized as the substrates (Table 4.5b).

Table 4.5 Substrate Scope of aromatic alkynes and methyl arene [a]

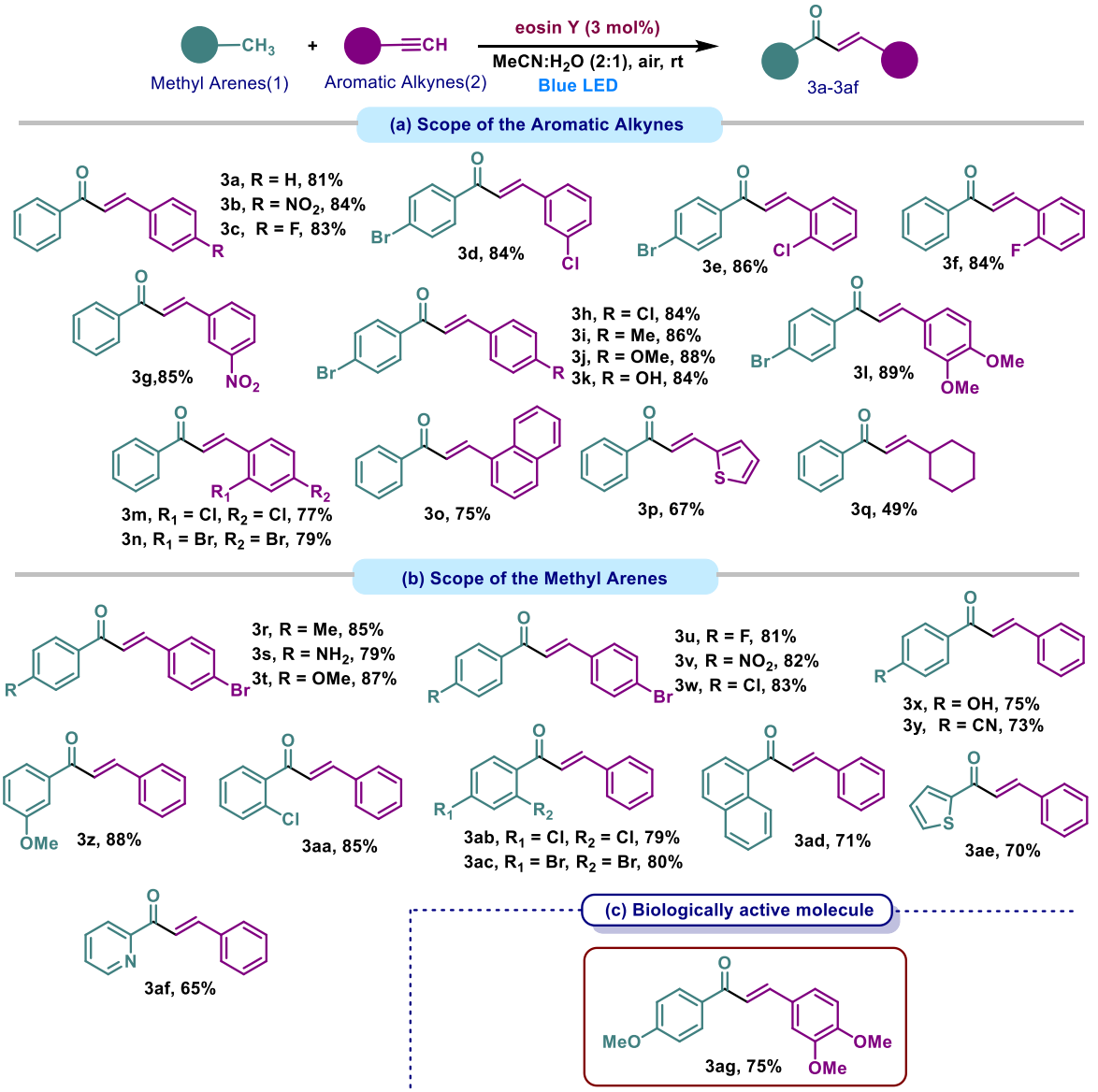

[a]Reaction Condition: methyl arene (0.25 mmol), aromatic alkynes (0.25 mmol), eosin Y (3 mol %), solvent (5 mL), blue LED (18 h) under open air at room temperature.

Methyl arene with various electron-donating substituents, including methyl, amino, methoxy, and hydroxyl groups, were well employed on phenylacetylene to produce chalcones in yields of 79-87%, 75% **(3r-3t, 3x),** respectively. Utilizing methyl arene with

electron-withdrawing substituents such as fluoro, nitro, chloro, and cyano group as the substrates, the hydroacylation process still went smoothly **(3u-3w, 3y)**. Regardless of the ortho- or meta-substituents used, the process produced **3aa and 3z** in 85% and 88% yields, respectively. The di-substituted and naphthalene ring-substituted methyl arene produced the anticipated chalcone derivatives **3ab-3ac and 3ad** in good 79-80%, and 71% yields, respectively. Heteroaromatic methyl arenes were well tolerated to give the acylated product in 70, and 65% yield **(3ae, and 3af)**. The strategy was biocompatible and was employed to create metachalcone in 75% yield **(3ag)**.

4.3 Control Experiment

A series of control experiments were carried out to reveal the hydroacylation process mechanistically. We studied the UV-visible spectra of the photocatalyst eosin Y, reactants, and reaction mixture (Figure 4.2). The outcomes demonstrated that the eosin Y and the reaction mixture could absorb blue light. The following step involved conducting a Stern−Volmer fluorescence quenching experiment on photocatalyst PC I in the presence of varying concentrations of toluene **1a** (Figure 4.3a). It was evident that toluene **1a** had a quenching impact on the excited photocatalysts (PC I*) emission, which indicated that direct interaction between PC I* and **1a** initiated the oxygenation process (Figure 4.4).

Additionally, intermediate A successfully quenched the excited state of PC I, indicating a direct interaction between PC I* and intermediate **A** (Figure 4.3b). Furthermore, visible-light ON-OFF experiments showed that the hydroxylation reaction was interrupted in the dark and resumed upon further irradiation, confirming that light was required throughout the reaction (Figure 4.5).

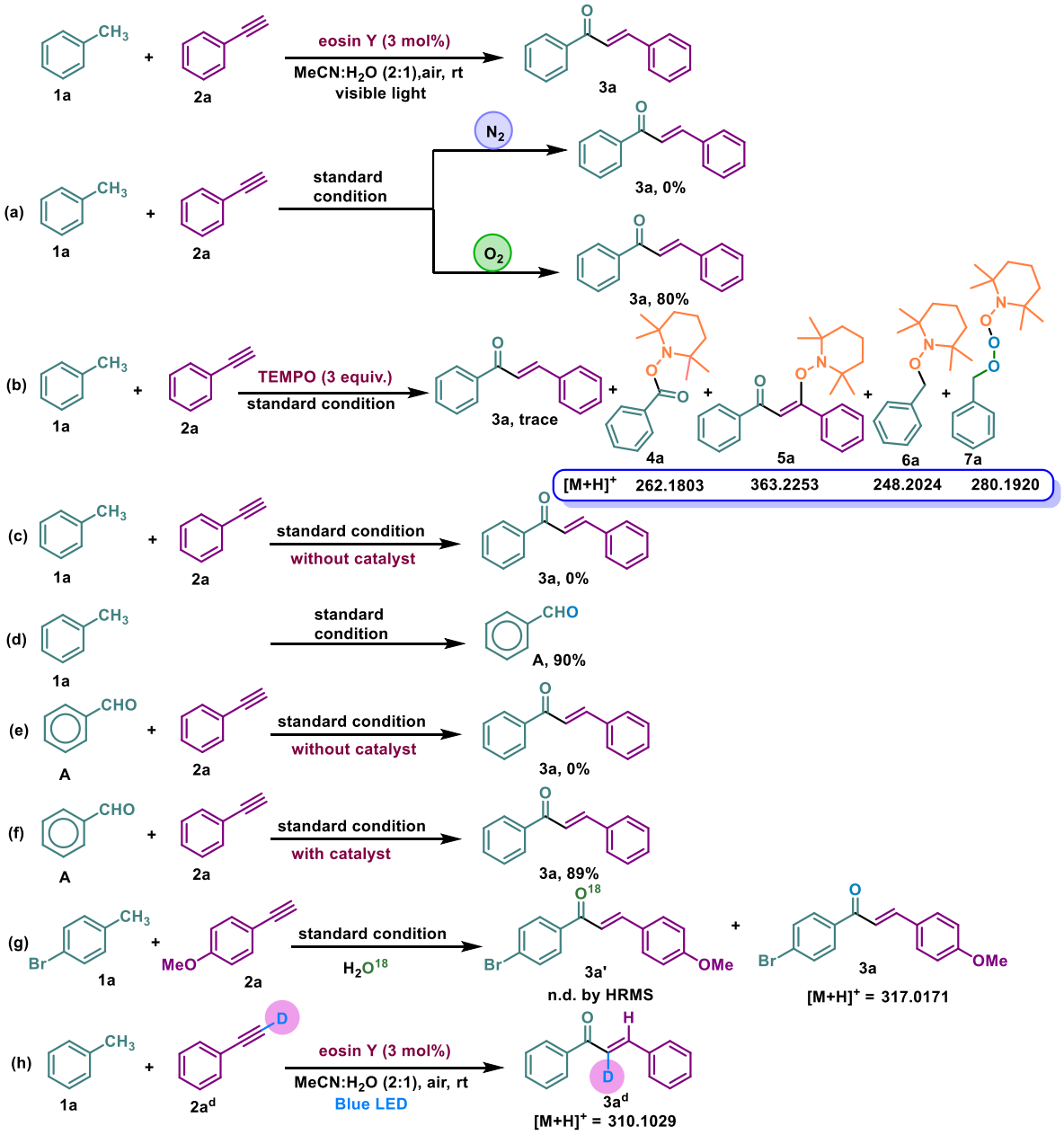

Scheme 4.3 Mechanistic Investigation

As shown in Scheme 4.3, the reaction could not create the desired product **3a** in an N_2 atmosphere, demonstrating the significance of O_2 to the reaction's success. It was also found that the reaction under oxygen gave essentially identical yield as under an air environment.

These findings suggested that this transition may depend significantly on the atmospheric oxygen, or O_2 generated in situ from H_2O_2 (Scheme 4.3a). We observed a significant suppression of the yields of product **3a** when the model reaction mixture was incorporated with a radical scavenger, 2,2,6,6-tetramethylpiperidin-1-oxyalkyl (TEMPO) (Scheme 4.3b). The generation of corresponding adducts **4a**, **5a, 6a, and 7a** of radical trapping was confirmed using HRMS data. The outcome confirms acyl radical formation and the reaction adheres to the free radical mechanism. There was no yield of product in the absence of the photocatalyst, demonstrating the significance of the catalyst (Scheme 4.3c). We were able to isolate intermediate **A** (Scheme 4.3d), which was detected by ^{1}H and ^{13}C NMR spectra. The reaction of **2a** with intermediate **A** (Scheme 4.3e and 4.3f) implicated the active participation of photocatalyst in the following step. To definitively ascertain whether the oxygen atom responsible for the oxidation of toluene originates from air or water, an isotope-labeling experiment was conducted in the presence of H_2O^{18}. However, no isotope-labeled product was observed (Scheme 4.3g). The observation rules out the involvement of oxygen from water molecules. A deuterium labeling experiment was conducted (Scheme 4.3h). The inclusion of "D" in product **3a^{d}** indicates that the proton of phenylacetylene stays intact.

4.3.1 UV-Vis absorption experiment

The sample was prepared by dissolving **1a, 2a**, and a mixture (**1a**+**2a**+eosin Y) in ethanol solvent [Conc. reaction mixture = 1.25×10^{-4}mol/L]. The absorption was measured, and the result is shown in Figure 4.2.

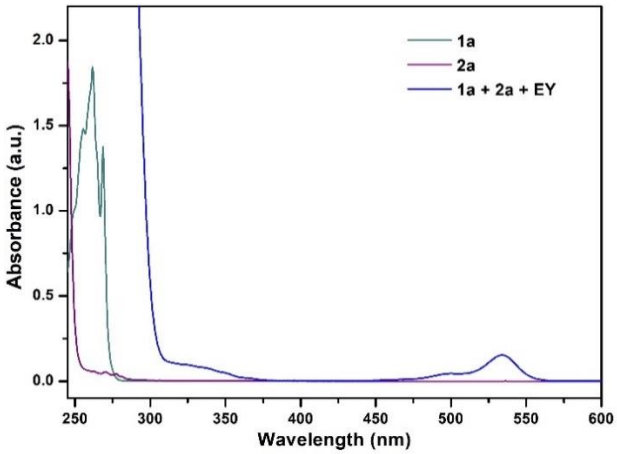

Figure 4.2 UV-Vis absorption spectra of (**1a**+**2a**)

4.3.2 Stern-Volmer Fluorescence Quenching Studies

The solution of **1a** in ethanol was added to the appropriate amount of eosin Y (EY) in a fluorescence experiment. The addition of **1a** was repeated 5 consecutive times. After each addition, we recorded the emission spectra. The solutions were excited at 551 nm, and the emission was acquired from 0 nm to 650 nm. The result shown in Figure 4.3a indicates that **1a** quenches the excited state of EY and its emission. The same was repeated for fluorescence quenching of eosin Y with Intermediate **A**, shown in Figure 4.3b.

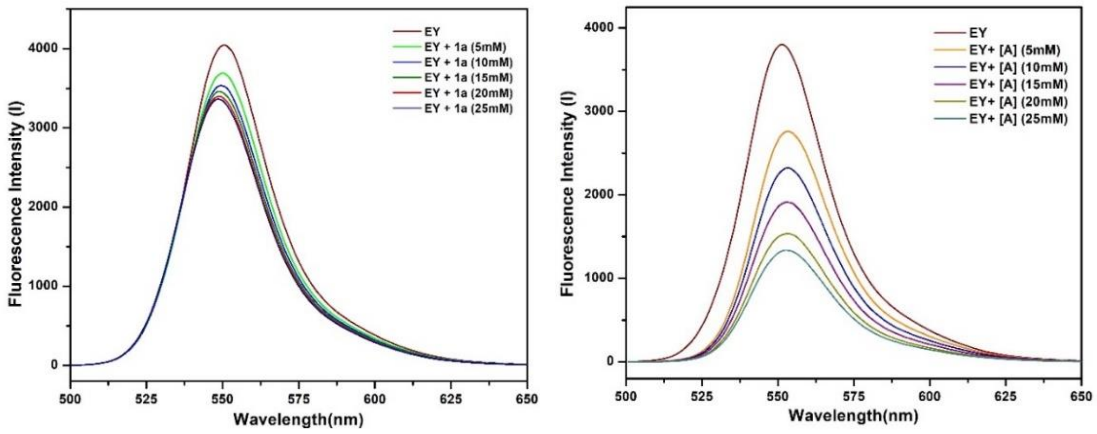

Figure 4.3 a, b The fluorescence emission spectra of EY with quencher **1a**, and **A**

The Stern-Volmer plot (Figure 4.4a, and b) indicated a linear relationship between the quencher concentrations and the ratio I_0/I. The Stern-Volmer constant K_{SV} was calculated using equation 1.

$I_0/I = 1 + K_{SV}[Q]$ …….**Eq. 1**

Where I_0 = the intensity of fluorescence of EY, without a quencher

I = the intensity of fluorescence of EY, with a quencher

[Q] = concentration of the quencher

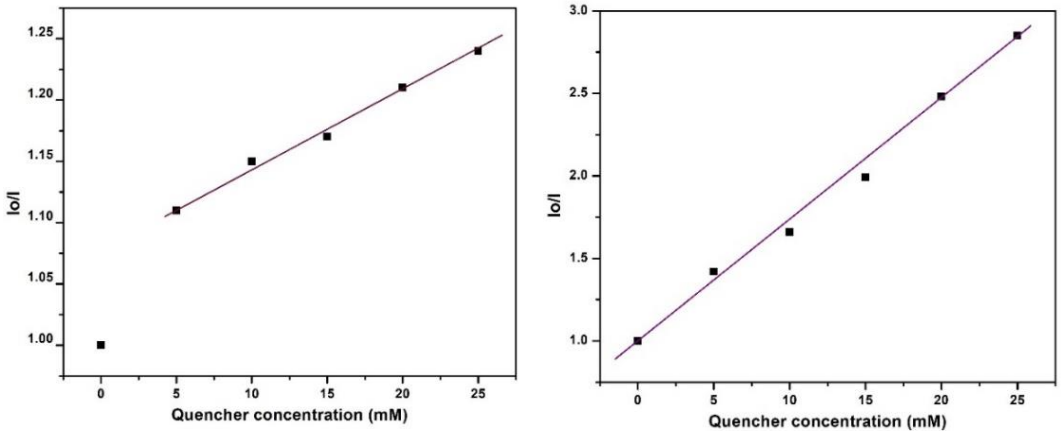

Figure 4.4 a Stern-Volmer plot of EY with different conc. of quencher **1a**
b Stern-Volmer plot of EY with different conc. of quencher **A**

4.3.3 ON-OFF Experiments

Under the prescribed conditions, a reaction between **1a** and **2a** was carried out on a scale of 0.25 mmol. Sequential periods of stirring the reaction mixture in the presence of visible light (blue LED) and then stirring in the absence of light were conducted. Each time a time point was reached, one reaction system was suspended, and it was later purified using column chromatography to yield the appropriate products **3a**. Using the product's weight, the yield of **3a** was calculated (Figure 4.5).

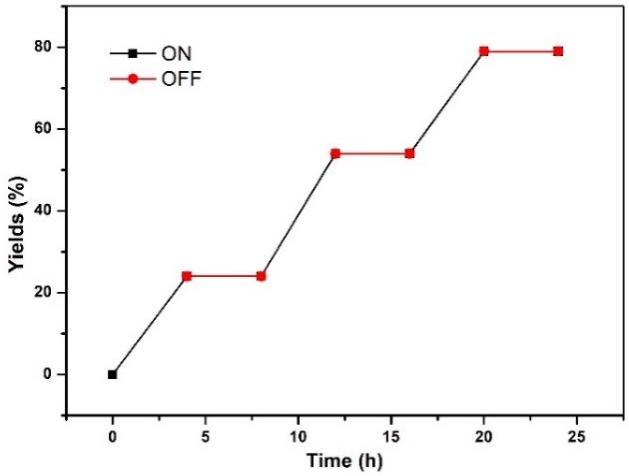

Figure 4.5 Light-Dark cycle experiment

4.4 Proposed Mechanism

Based on the above control experiments and literature reviews [49,53-55], we suggested a plausible mechanism for photo-induced hydroacylation via C(sp^3)-H activation (Scheme 4.4). First of all, methyl arene gets converted into intermediate **A** (already discussed in our previous work, ref-49). When exposed to blue light, eosin Y (PC I) transforms to its excited state (PC I*), which removes aldehydic hydrogen from intermediate **A**, resulting in the acyl radical intermediate **B**. This intermediate **B** attacks phenyl acetylene **2a** to form radical intermediate **C**. Radical intermediate **C** undergoes the reverse HAT (RHAT) cycle to mediate the recovery of PC and give the desired product **3a**. (pathway a) Alternatively, a HAT process involving another benzaldehyde molecule and radical **C** could be employed to attain the desired outcome **3a**. Subsequently, an RHAT between an acyl radical **B** and PC I-H could regenerate the ground state PC I. (pathway b)

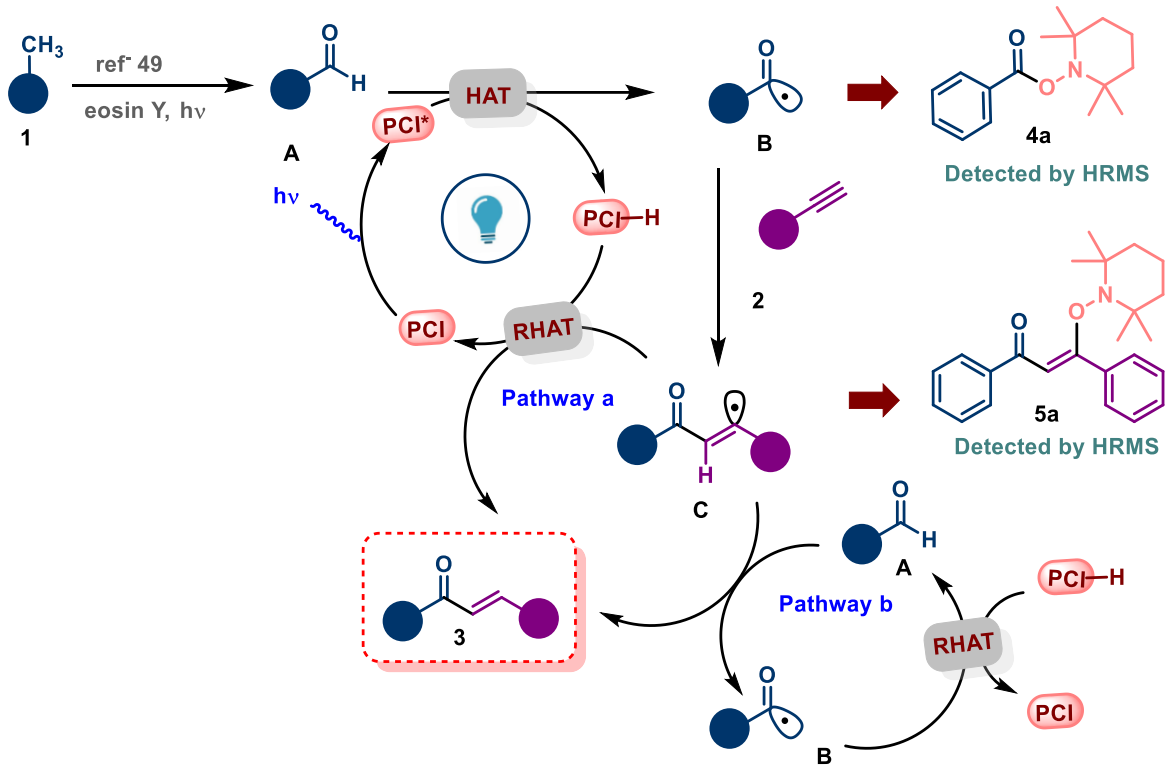

Scheme 4.4 Plausible mechanism

4.5 Conclusions

In conclusion, we have developed the first method for hydroacylating terminal alkynes employing C(sp^3)-H functionalized methyl arenes as the acylating agent using metal-free photoredox catalysis in a more environmentally friendly solvent. Hydroacylation allows a wide variety of chalcones to be easily produced in good to outstanding yields with strong functional group tolerance. The current approach is cost-effective, atom-efficient, ecologically benign, and tolerates various functional groups. The detailed mechanistic analysis showed that a metal-free catalyst catalyzes the process and follows a radical pathway, and the development of intermediates indicates C-H functionalization.

4.6 Experimental Procedures

4.6.1 General procedure for the preparation of chalcones

A 25 mL RB flask equipped with a magnetic stirring bar was charged with methyl arenes **1** (0.25 mmol, 1.0 equiv.), eosin Y (3 mol %,) and solvent (MeCN:H_2O, v/v-2:1, 5 mL). The mixture was then stirred at room temperature and irradiated with blue LED light strips for 6 h under the open air. After that phenylacetylene derivatives **2** (0.25 mmol, 1.0 equiv.) were added to the reaction mixture. The progress of the reaction was monitored via TLC. After completion of the reaction, the resultant mixture was extracted with ethyl acetate (20 mL × 3), and the resulting organic layer was collected and dried with $MgSO_4$. Following the solvent's removal under reduced pressure, the crude product was purified by silica gel column chromatography with 15% ethyl acetate/ n-hexane to get the desired product.

4.6.2 1 mmol Scale Synthesis of Product 3a

A 100 mL RB flask equipped with a magnetic stirring bar was charged with toluene **1a** (0.107 mL, 1 mmol, 1.0 equiv.), eosin Y (41.5mg, 3 mol %,) and solvent (MeCN:H_2O, v/v-2:1, 20 mL). The mixture was then stirred at room temperature and irradiated with blue LED light strips for 6 h under the open air. After that phenylacetylene **2a** (0.110 mL, 1 mmol, 1.0 equiv.) was added to the reaction mixture. The progress of the reaction was monitored via TLC. After completion of the reaction, the resultant mixture was extracted with ethyl acetate (30 mL × 3), and the resulting organic layer was collected and dried with $MgSO_4$. Following

the solvent's removal under reduced pressure, the crude product was purified by silica gel column chromatography with ethyl acetate/ *n*-hexane (1:7) to get the desired product **3a** (162.4mg, 78%).

4.7 Characterization of compounds

(E)-Chalcone (3a)

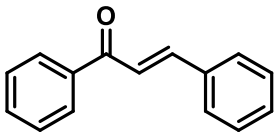

81% yield; creamy yellow solid; m.p. 57-59^{o}C; **^{1}H NMR** (500 MHz, $CDCl_3$) δ 8.07 – 8.04 (m, 2H), 7.84 (d, *J* = 15.7 Hz, 1H), 7.68 (dd, *J* = 6.4, 3.2 Hz, 2H), 7.62 (t, *J* = 7.4 Hz, 1H), 7.58 – 7.52 (m, 3H), 7.45 (dd, *J* = 5.0, 1.8 Hz, 3H). **^{13}C NMR** (126 MHz, $CDCl_3$) δ 190.6, 144.9, 138.2, 134.9, 132.8, 130.5, 128.9, 128.6, 128.5, 128.4, 122.2. **HRMS** (ESI) m/z: $[M+H]^+$ calculated for $C_{15}H_{13}O$: 209.0966; found: 209.0964.

(E)-3-(4-Nitrophenyl)-1-phenylprop-2-en-1-one (3b)

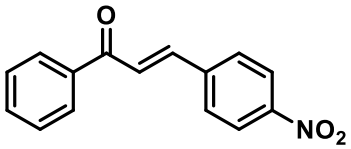

84% yield; light blue solid; m.p. 110-111^{o}C; **^{1}H NMR** (500 MHz, $CDCl_3$) δ 8.00 (d, *J* = 8.7 Hz, 2H), 7.84 (d, *J* = 15.7 Hz, 1H), 7.69 – 7.66 (m, 2H), 7.51 (dd, *J* = 12.2, 3.5 Hz, 3H), 7.47 – 7.44 (m, 3H). **^{13}C NMR** (126 MHz, $CDCl_3$) δ 189.2, 145.4, 139.2, 136.5, 134.7, 130.7, 129.9, 129.0, 128.9, 128.5, 121.5. **HRMS** (ESI) m/z: $[M+H]^+$ calculated for $C_{15}H_{12}NO_3$: 254.0817; found: 254.0818.

(E)-3-(4-Fluorophenyl)-1-phenylprop-2-en-1-one (3c)

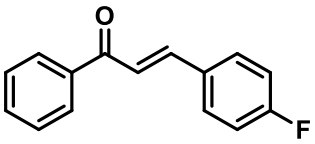

83% yield; light yellow solid; m.p. 104-106°C; **^{1}H NMR** (500 MHz, $CDCl_3$) δ 8.09 (dd, *J* = 8.9, 5.4 Hz, 2H), 7.84 (d, *J* = 15.7 Hz, 1H), 7.69 – 7.66 (m, 2H), 7.53 (d, *J* = 15.7 Hz, 1H), 7.47 – 7.44 (m, 3H), 7.21 (t, *J* = 8.6 Hz, 2H). **^{13}C NMR** (126 MHz, $CDCl_3$) δ 188.9, 166.6, 164.62, 145.1, 134.8, 131.1 (d, J = 9.2 Hz), 130.7, 129.1, 128.5, 121.6, 115.8, 115.7. **^{19}F NMR** (471 MHz, $CDCl_3$) δ -105.6. **HRMS** (ESI) m/z: [M+H] + calculated for $C_{15}H_{12}FO$: 227.0872; found: 227.0870.

(E)-1-(4-Bromophenyl)-3-(3-chlorophenyl)prop-2-en-1-one (3d)

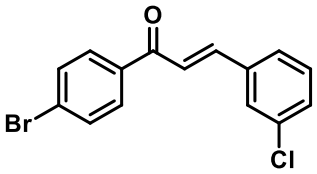

84% yield; yellowish brown solid; m.p. 91-92°C; **^{1}H NMR** (500 MHz, DMSO-d_6) δ 8.14 (d, *J* = 8.6 Hz, 2H), 8.10 (s, 1H), 8.03 (d, *J* = 15.6 Hz, 1H), 7.84 (d, *J* = 7.3 Hz, 1H), 7.80 (d, *J* = 8.6 Hz, 2H), 7.74 (d, *J* = 15.6 Hz, 1H), 7.54 – 7.47 (m, 2H). **^{13}C NMR** (126 MHz, DMSO-d_6) δ 188.6, 143.2, 137.3, 136.8, 134.3, 132., 131.1, 130.7, 128.5, 128.0, 123.7. **HRMS** (ESI) m/z: $[M+H]^+$ calculated for $C_{15}H_{11}BrClO$: 320.9682; found: 320.9685.

(E)-1-(4-Bromophenyl)-3-(2-chlorophenyl)prop-2-en-1-one (3e)

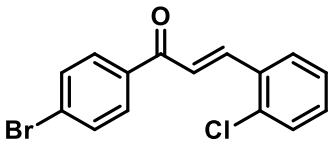

86% yield; yellowish brown solid; m.p. 98-99°C; **^{1}H NMR** (500 MHz, $CDCl_3$) δ 7.92 (d, *J* = 8.6 Hz, 2H), 7.77 (d, *J* = 15.7 Hz, 1H), 7.70 – 7.64 (m, 3H), 7.51 (dd, *J* = 13.8, 11.7 Hz, 2H), 7.44 – 7.37 (m, 2H). **^{13}C NMR** (126 MHz, $CDCl_3$) δ 188.9, 143.6, 136.6, 136.5, 135.1, 132.0, 130.6, 130.3, 130.1, 128.2, 127.9, 126.9, 122.6. **HRMS** (ESI) m/z: $[M+H]^+$ calculated for $C_{15}H_{11}OBrCl$: 320.9682; found: 320.9683.

(E)-3-(2-Fluorophenyl)-1-phenylprop-2-en-1-one (3f)

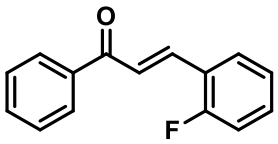

84% yield; light yellow solid; m.p. 107-109°C; **^{1}H NMR** (500 MHz, $CDCl_3$) δ 8.04 (d, *J* = 7.1 Hz, 2H), 7.80 (d, *J* = 15.7 Hz, 1H), 7.67 (dd, *J* = 8.5, 5.4 Hz, 2H), 7.62 (t, *J* = 6.8 Hz, 1H), 7.54 (t, *J* = 7.6 Hz, 2H), 7.49 (d, *J* = 15.7 Hz, 1H), 7.16 – 7.12 (m, 2H). **^{13}C NMR** (126 MHz, $CDCl_3$) δ 190.3, 165.1, 163.1, 143.5, 138.2, 132.8, 131.2, 130.3 (d, J = 8.5 Hz), 128.7, 128.5, 121.8, 116.2, 116.1. **^{19}F NMR** (471 MHz, $CDCl_3$) δ -109.1. **HRMS** (ESI) m/z: $[M+H]^+$ calculated for $C_{15}H_{12}OF$: 227.0872; found: 227.0874.

(E)-3-(3-Nitrophenyl)-1-phenylprop-2-en-1-one (3g)

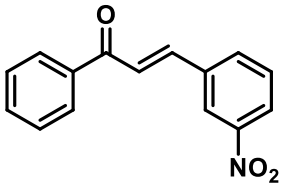

85% yield; light yellow solid; m.p. 115-117°C; **^{1}H NMR** (500 MHz, $CDCl_3$) δ 8.54 (s, 1H), 8.30 (dd, *J* = 8.2, 1.4 Hz, 1H), 7.94 (d, *J* = 8.5 Hz, 3H), 7.87 (d, *J* = 15.7 Hz, 1H), 7.82 (d, *J* = 8.7 Hz, 1H), 7.71 (d, *J* = 8.6 Hz, 2H), 7.64 (dd, *J* = 11.8, 9.6 Hz, 2H). **^{13}C NMR** (126 MHz, $CDCl_3$) δ 188.5, 142.2, 136.5, 136.3, 134.4, 132.1, 130.1, 129.6, 128.6, 124.8, 124.0, 122.3. **HRMS** (ESI) m/z: $[M+H]^+$ calculated for $C_{15}H_{12}NO_3$: 254.0817; found: 254.0820.

(E)-1-(4-Bromophenyl)-3-(4-chlorophenyl)prop-2-en-1-one (3h)

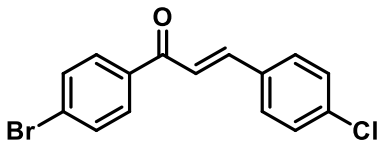

84% yield; yellowish brown solid; m.p. 97-98°C; **^{1}H NMR** (500 MHz, $CDCl_3$) δ 7.90 (d, *J* = 8.5 Hz, 2H), 7.78 (d, *J* = 15.7 Hz, 1H), 7.67 (d, *J* = 8.5 Hz, 2H), 7.59 (d, *J* = 8.5 Hz, 2H), 7.47 (d, *J* = 15.7 Hz, 1H), 7.42 (d, *J* = 8.5 Hz, 2H). **^{13}C NMR** (126 MHz, $CDCl_3$) δ 189.1, 143.9, 136.7, 136.7, 133.2, 132.0, 130.0, 129.6, 129.3, 128.1, 121.8. **HRMS** (ESI) m/z: $[M+H]^+$ calculated for $C_{15}H_{11}BrClO$: 320.9682; found: 320.9680.

(E)-1-(4-Bromophenyl)-3-(p-tolyl)prop-2-en-1-one (3i)

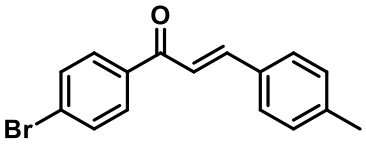

86% yield; yellow solid; m.p. 102-103°C; **^{1}H NMR** (500 MHz, $CDCl_3$) δ 7.91 (d, *J* = 8.5 Hz, 2H), 7.82 (d, *J* = 15.7 Hz, 1H), 7.67 (d, *J* = 8.6 Hz, 2H), 7.57 (d, *J* = 8.1 Hz, 2H), 7.46 (d, *J* = 15.7 Hz, 1H), 7.26 (d, *J* = 8.0 Hz, 2H), 2.42 (s, 3H). **^{13}C NMR** (126 MHz, $CDCl_3$) δ 189.5, 145.5, 141.4, 137.1, 131.9, 130.0, 129.8, 128.9, 127.7, 120.5, 21.6. **HRMS** (ESI) m/z: $[M+H]^+$ calculated for $C_{16}H_{14}BrO$: 301.0228; found: 301.0229.

(E)-1-(4-Bromophenyl)-3-(4-methoxyphenyl)prop-2-en-1-one (3j)

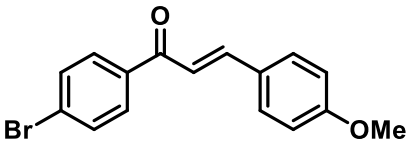

88% yield; yellowish brown solid; m.p. 100-101°C; **^{1}H NMR** (500 MHz, DMSO-d_6) δ 8.09 (d, *J* = 8.6 Hz, 2H), 7.87 (d, *J* = 8.8 Hz, 2H), 7.81 – 7.72 (m, 4H), 7.03 (d, *J* = 8.8 Hz, 2H), 3.83 (s, 3H). **^{13}C NMR** (126 MHz, DMSO-d_6) δ 188.6, 162.0, 145.0, 137.3, 132.3, 131.4, 130.9, 127.7, 127.5, 119.6, 114.9, 55.9. **HRMS** (ESI) m/z: $[M+H]^+$ calculated for $C_{16}H_{14}BrO_2$: 317.0177; found: 317.0171.

(E)-1-(4-Bromophenyl)-3-(4-hydroxyphenyl)prop-2-en-1-one(3k)

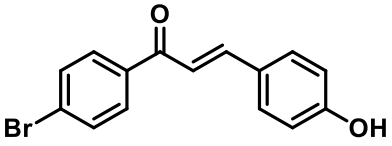

84% yield; yellowish solid; m.p. 81-83°C; **^{1}H NMR** (500 MHz, $CDCl_3$) δ 9.64 (s, 1H), 7.91 (d, *J* = 8.5 Hz, 2H), 7.79 (d, *J* = 15.7 Hz, 1H), 7.68 (d, *J* = 8.5 Hz, 2H), 7.60 (d, *J* = 8.5 Hz, 2H), 7.47 (d, *J* = 15.7 Hz, 1H), 7.42 (d, *J* = 8.5 Hz, 2H). **^{13}C NMR** (126 MHz, $CDCl_3$) δ 189.1, 157.3, 143.9, 136.7, 133.2, 131.9, 130.0, 129.6, 129.3, 128.1, 121.9. **HRMS** (ESI) m/z: [M+H] + calculated for $C_{15}H_{12}BrO_2$: 303.0020; found: 303.0023.

(E)-1-(4-Bromophenyl)-3-(3,4-dimethoxyphenyl)prop-2-en-1-one (3l)

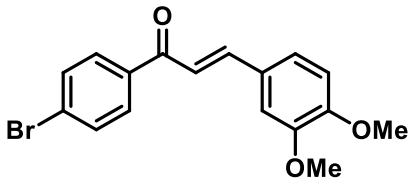

89% yield; yellowish brown solid; m.p. 98-99°C; **^{1}H NMR** (500 MHz, $CDCl_3$) δ 7.90 (d, *J* = 8.4 Hz, 2H), 7.79 (d, *J* = 15.6 Hz, 1H), 7.67 (d, *J* = 8.3 Hz, 2H), 7.35 (d, *J* = 15.6 Hz, 1H), 7.26 (dd, *J* = 8.3, 1.9 Hz, 1H), 7.18 (d, *J* = 1.8 Hz, 1H), 6.93 (d, *J* = 8.3 Hz, 1H), 3.98 (s, 3H), 3.96 (s, 3H). **^{13}C NMR** (126 MHz, $CDCl_3$) δ 189.5, 151.7, 149.3, 145.6, 137.2, 131.9, 129.9, 127.7, 123.3, 119.5, 111.9, 110.2, 56.0, 56.0. **HRMS** (ESI) m/z: $[M+H]^+$ calculated for $C_{17}H_{16}BrO_3$: 347.0283; found: 347.0280.

(E)-3-(2,4-Dichlorophenyl)-1-phenylprop-2-en-1-one (3m)

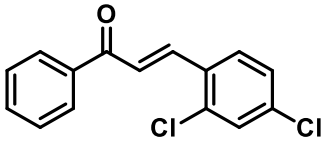

77% yield; yellowish brown solid; m.p.; 133-134°C; **^{1}H NMR** (500 MHz, $CDCl_3$) δ 8.13 (d, *J* = 15.8 Hz, 1H), 8.06 – 8.02 (m, 2H), 7.71 (d, *J* = 8.5 Hz, 1H), 7.63 (t, *J* = 6.8 Hz, 1H), 7.54 (t, *J* = 7.6 Hz, 2H), 7.50 (dd, *J* = 8.9, 6.8 Hz, 2H), 7.33 (d, *J* = 6.8 Hz, 1H). **^{13}C NMR** (126 MHz, $CDCl_3$) δ 190.1, 139.4, 137.8, 136.5, 136.1, 133.1, 131.9, 130.2, 128.7, 128.6, 128.5, 127.6, 125.1. **HRMS** (ESI) m/z: $[M+H]^+$ calculated for $C_{15}H_{11}Cl_2O$: 277.0187; found: 277.0185.

(E)-3-(2,4-Dibromophenyl)-1-phenylprop-2-en-1-one (3n)

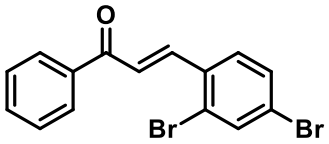

79% yield; yellowish brown solid; m.p. 142-143°C; **^{1}H NMR** (500 MHz, $CDCl_3$) δ 8.13 (d, *J* = 15.8 Hz, 1H), 8.06 – 8.02 (m, 2H), 7.71 (d, *J* = 8.5 Hz, 1H), 7.63 (t, *J* = 6.8 Hz, 1H), 7.54 (t, *J* = 7.6 Hz, 2H), 7.50 (dd, *J* = 8.9, 6.8 Hz, 2H), 7.33 (d, *J* = 6.8 Hz, 1H). **^{13}C NMR** (126 MHz, $CDCl_3$) δ 190.2, 139.4, 137.8, 136.5, 136.1, 133.1, 131.9, 130.2, 128.7, 128.6, 128.5, 127.6, 125.1. **HRMS** (ESI) m/z: $[M+H]^+$ calculated for $C_{15}H_{11}Br_2O$: 364.9177; found: 364.9180.

(E)-3-(Naphthalen-1-yl)-1-phenylprop-2-en-1-one (3o)

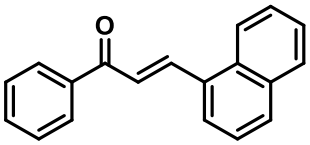

75% yield; yellowish brown solid; m.p. 178-179°C; **^{1}H NMR** (500 MHz, DMSO-d_6) δ 8.58 (d, *J* = 15.4 Hz, 1H), 8.28 (dd, *J* = 15.3, 7.8 Hz, 2H), 8.23 – 8.19 (m, 2H), 8.08 (d, *J* = 8.2 Hz, 1H), 8.05 – 8.00 (m, 2H), 7.70 (dd, *J* = 15.4, 8.0 Hz, 2H), 7.62 (dt, *J* = 10.0, 7.8 Hz, 4H). **^{13}C NMR** (126 MHz, DMSO-d_6) δ 189.6, 140.4, 138.0, 133.8, 133.7, 131.8, 131.7, 131.3, 129.3, 129.3, 129.1, 127.7, 126.8, 126.2, 126.2, 125.1, 123.5. **HRMS** (ESI) m/z: $[M+H]^+$ calculated for $C_{19}H_{15}O$: 259.1123; found: 259.1120.

(E)-1-Phenyl-3-(thiophen-2-yl)prop-2-en-1-one (3p)

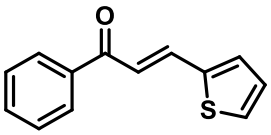

67% yield; light yellow solid; m.p. 78-80°C; **^{1}H NMR** (500 MHz, $CDCl_3$) δ 8.05 – 8.01 (m, 2H), 7.97 (d, *J* = 15.3 Hz, 1H), 7.62 – 7.58 (m, 1H), 7.53 (dd, *J* = 10.7, 4.3 Hz, 2H), 7.45 (d, *J* = 5.1 Hz, 1H), 7.39 (d, *J* = 3.6 Hz, 1H), 7.36 (d, *J* = 15.4 Hz, 1H), 7.13 – 7.10 (m, 1H). **^{13}C NMR** (126 MHz, $CDCl_3$) δ 189.9, 140.4, 138.2, 137.2, 132.8, 132.1, 128.8, 128.6, 128.4, 128.4, 120.8. **HRMS** (ESI) m/z: $[M+H]^+$ calculated for $C_{13}H_{11}SO$: 215.0531; found: 215.0535.

(E)-3-Cyclohexyl-1-phenylprop-2-en-1-one (3q)

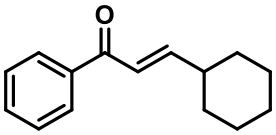

49% yield; yellowish liquid; **^{1}H NMR** (500 MHz, $CDCl_3$) δ 7.96 (d, *J* = 7.7 Hz, 1H), 7.88 (d, *J* = 7.6 Hz, 2H), 7.48 (t, *J* = 7.5 Hz, 2H), 6.96 (d, *J* = 15.1 Hz, 1H), 6.50 (dd, *J* = 15.1, 10.2 Hz, 1H), 3.07 – 2.99 (m, 1H), 1.93 – 1.81 (m, 1H), 1.06 (t, *J* = 7.0 Hz, 1H), 0.99 – 0.94 (m, 2H). **^{13}C NMR** (126 MHz, $CDCl_3$) δ 188.7, 154.1, 136.9, 136.0, 131.7, 131.3, 127.2, 121.7, 43.7, 42.7, 36.7, 25.9. **HRMS** (ESI) m/z: $[M+H]^+$ calculated for $C_{15}H_{19}O$: 214.1358; found: 214.1255.

(E)-3-(4-Bromophenyl)-1-(p-tolyl)prop-2-en-1-one (3r)

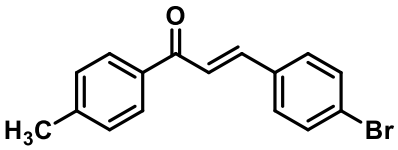

85% yield; creamy yellow solid; m.p. 87-88°C; **^{1}H NMR** (500 MHz, $CDCl_3$) δ 7.91 (d, *J* = 8.5 Hz, 2H), 7.82 (d, *J* = 15.7 Hz, 1H), 7.66 (d, *J* = 8.5 Hz, 2H), 7.56 (d, *J* = 8.1 Hz, 2H), 7.45 (d, *J* = 15.7 Hz, 1H), 7.26 (d, *J* = 7.9 Hz, 2H), 2.42 (s, 3H). **^{13}C NMR** (126 MHz, $CDCl_3$) δ 189.5, 145.5, 141.4, 137.1, 131.9, 130.0, 129.7, 128.5, 127.7, 120.5, 21.5. **HRMS** (ESI) m/z: $[M+H]^+$ calculated for $C_{16}H_{14}BrO$: 301.0228; found: 301.0225.

(E)-1-(4-Aminophenyl)-3-(4-bromophenyl)prop-2-en-1-one (3s)

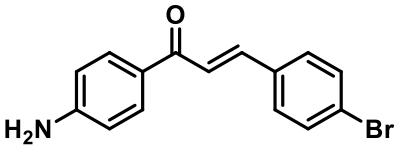

79% yield; yellowish brown solid; m.p. 117-118°C; **^{1}H NMR** (500 MHz, $CDCl_3$) δ 7.92 (d, *J* = 8.6 Hz, 2H), 7.77 (d, *J* = 15.7 Hz, 1H), 7.68 (dd, *J* = 12.6, 5.7 Hz, 3H), 7.52 (d, *J* = 7.7 Hz, 1H), 7.50 (d, *J* = 15.7 Hz, 1H), 7.44 – 7.37 (m, 2H), 5.22 (s, 2H). **^{13}C NMR** (126 MHz, $CDCl_3$) δ 188.9, 143.6, 136.6, 136.4, 135.1, 132.0, 130.4, 130.3, 129.9, 128.2, 127.9, 126.9, 122.6. **HRMS** (ESI) m/z: $[M+H]^+$ calculated for $C_{15}H_{13}BrNO$: 302.0180; found: 302.0185.

(E)-1-(4-Methoxyphenyl)-3-phenylprop-2-en-1-one (3t)

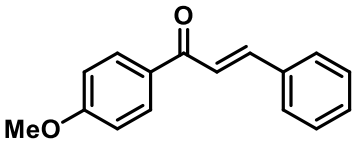

87% yield; creamy yellow solid; m.p. 80-81°C; **^{1}H NMR** (500 MHz, DMSO-d_6) δ 8.18 (d, *J* = 8.9 Hz, 2H), 7.95 (d, *J* = 15.6 Hz, 1H), 7.89 (dd, *J* = 7.2, 2.2 Hz, 2H), 7.72 (d, *J* = 15.6 Hz, 1H), 7.46 (d, *J* = 1.7 Hz, 3H), 7.10 (d, *J* = 8.9 Hz, 2H), 3.88 (s, 3H). **^{13}C NMR** (126 MHz, DMSO-d_6) δ 187.8, 163.7, 143.6, 135.3, 131.4, 130.9, 129.4, 129.3, 122.5, 114.5, 56.1. **HRMS** (ESI) m/z: $[M+H]^+$ calculated for $C_{16}H_{15}O_2$: 239.1072; found: 239.1073.

(E)-3-(4-Bromophenyl)-1-(4-fluorophenyl)prop-2-en-1-one (3u)

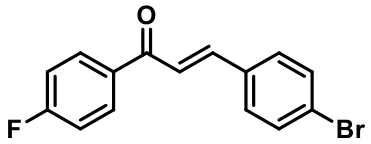

81% yield; creamy solid; m.p. 89-91°C; **^{1}H NMR** (500 MHz, $CDCl_3$) δ 7.90 (d, *J* = 8.6 Hz, 2H), 7.78 (d, *J* = 15.7 Hz, 1H), 7.67 (d, *J* = 8.6 Hz, 2H), 7.60 (d, *J* = 8.4 Hz, 2H), 7.47 (d, *J* = 15.7 Hz, 1H), 7.42 (d, *J* = 8.4 Hz, 2H). **^{13}C NMR** (126 MHz, $CDCl_3$) δ 189.1, 143.8, 136.7 (d, J = 7.5 Hz), 133.2, 132.0, 130.0, 129.6, 129.3, 128.1, 121.9. **^{19}F NMR** (471 MHz, $CDCl_3$) δ -115.8, -115.8, -115.8. **HRMS** (ESI) m/z: $[M+H]^+$ calculated for $C_{15}H_{11}BrFO$: 304.9977; found: 304.9975.

(E)-3-(4-Bromophenyl)-1-(4-nitrophenyl)prop-2-en-1-one (3v)

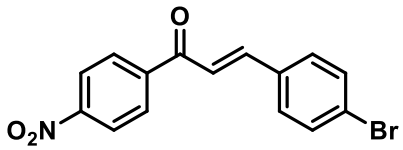

82% yield; yellowish brown solid; m.p. 134-136°C; **^{1}H NMR** (500 MHz, $CDCl_3$) δ 7.90 (d, *J* = 8.6 Hz, 2H), 7.78 (d, *J* = 15.7 Hz, 1H), 7.67 (d, *J* = 8.6 Hz, 2H), 7.60 (d, *J* = 8.4 Hz, 2H), 7.47 (d, *J* = 15.7 Hz, 1H), 7.42 (d, *J* = 8.5 Hz, 2H). **^{13}C NMR** (126 MHz, $CDCl_3$) δ 189.1, 143.9, 136.7, 136.7, 133.2, 132.1, 130.0, 129.6, 129.3, 128.1, 121.9. **HRMS** (ESI) m/z: $[M+H]^+$ calculated for $C_{15}H_{11}BrNO_3$: 331.9922; found: 331.9924.

(E)-3-(4-Bromophenyl)-1-(4-chlorophenyl)prop-2-en-1-one (3w)

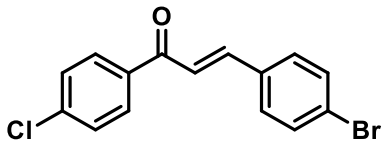

83% yield; creamy solid; m.p. 100-102°C; **^{1}H NMR** (500 MHz, $CDCl_3$) δ 7.91 (d, *J* = 8.5 Hz, 2H), 7.79 (d, *J* = 15.7 Hz, 1H), 7.68 (d, *J* = 8.5 Hz, 2H), 7.60 (d, *J* = 8.5 Hz, 2H), 7.47 (d, *J* = 15.7 Hz, 1H), 7.42 (d, *J* = 8.5 Hz, 2H). **^{13}C NMR** (126 MHz, $CDCl_3$) δ 189.1, 143.8, 136.7, 136.7, 133.2, 131.9, 130.0, 129.6, 129.3, 128.1, 121.8. **HRMS** (ESI) m/z: $[M+H]^+$ calculated for $C_{15}H_{11}BrClO$: 320.9682; found: 320.9683.

(E)-1-(4-Hydroxyphenyl)-3-phenylprop-2-en-1-one (3x)

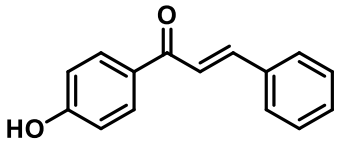

75% yield; yellowish brown solid; m.p. 77-79°C; **^{1}H NMR** (500 MHz, DMSO-d_6) δ 9.64 (s, 1H), 8.28 (d, *J* = 8.2 Hz, 1H), 8.02 (d, *J* = 15.5 Hz, 1H), 7.87 – 7.82 (m, 2H), 7.68 – 7.63 (m, 2H), 7.45 (d, *J* = 7.1 Hz, 3H), 6.90 (d, *J* = 8.5 Hz, 1H), 6.78 (t, *J* = 7.6 Hz, 1H). **^{13}C NMR** (126 MHz, DMSO-d_6) δ 196.5, 162.5, 145.7, 135.5, 131.2, 129.1, 127.2, 119.7, 116.1, 115.6. **HRMS** (ESI) m/z: $[M+H]^+$ calculated for $C_{15}H_{13}O_2$: 225.0915; found: 225.0918.

4-Cinnamoylbenzonitrile (3y)

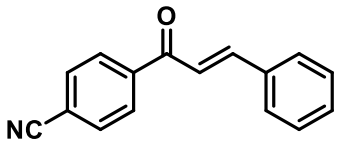

73% yield; creamy yellow solid; m.p. 110-113°C; **^{1}H NMR** (500 MHz, $CDCl_3$) δ 8.11 (d, *J* = 8.6 Hz, 2H), 7.85 (dd, *J* = 13.3, 12.2 Hz, 3H), 7.70 – 7.66 (m, 2H), 7.51 – 7.45 (m, 4H). **^{13}C NMR** (126 MHz, $CDCl_3$) δ 189.2, 146.6, 141.5, 134.4, 132.5, 131.2, 129.1, 128.8, 128.7, 121.2, 118.0, 116.00. **HRMS** (ESI) m/z: $[M+H]^+$ calculated for $C_{16}H_{12}NO$: 234.0919; found: 234.0918.

(E)-1-(3-Methoxyphenyl)-3-phenylprop-2-en-1-one (3z)

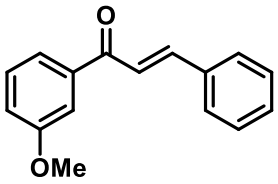

88% yield; yellowish brown solid; m.p. 75-76°C; **^{1}H NMR** (500 MHz, $CDCl_3$) δ 8.07 (d, *J* = 8.9 Hz, 2H), 7.83 (d, *J* = 15.7 Hz, 1H), 7.69 – 7.65 (m, 2H), 7.57 (d, *J* = 15.7 Hz, 1H), 7.47 – 7.44 (m, 1H), 7.43 (dd, *J* = 4.7, 1.8 Hz, 2H), 7.01 (d, *J* = 8.9 Hz, 2H), 3.92 (s, 3H). **^{13}C NMR** (126 MHz, $CDCl_3$) δ 188.8, 163.5, 143.9, 135.1, 131.1, 130.8, 130.3, 128.9, 128.4, 121.9, 113.8, 55.5. **HRMS** (ESI) m/z: $[M+H]^+$ calculated for $C_{16}H_{15}O_2$: 239.1072; found: 239.1070.

(E)-1-(2-Chlorophenyl)-3-phenylprop-2-en-1-one (3aa)

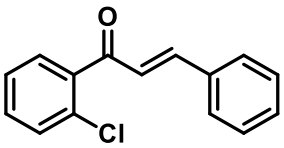

85% yield; creamy yellow solid; m.p. 63-65°C; **^{1}H NMR** (500 MHz, DMSO-d_6) δ 7.77 (dd, *J* = 7.6, 1.7 Hz, 2H), 7.61 – 7.55 (m, 3H), 7.51 (dd, *J* = 7.3, 1.5 Hz, 1H), 7.49 – 7.45 (m, 2H), 7.45 – 7.40 (m, 2H), 7.29 (d, *J* = 16.1 Hz, 1H). **^{13}C NMR** (126 MHz, DMSO-d_6) δ 193.7, 146.7, 139.1, 134.5, 132.3, 131.5, 130.6, 130.4, 129.7, 129.5, 129.3, 127.9, 126.7. **HRMS** (ESI) m/z: $[M+H]^+$ calculated for $C_{15}H_{12}ClO$: 243.0577; found: 243.0575.

(E)-1-(2,4-Dichlorophenyl)-3-phenylprop-2-en-1-one (3ab)

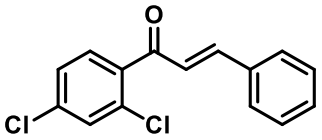

79% yield; yellowish brown solid; m.p. 128-129°C; **^{1}H NMR** (500 MHz, DMSO-d_6) δ 8.27 (d, *J* = 8.6 Hz, 1H), 8.20 – 8.16 (m, 2H), 8.01 (q, *J* = 15.6 Hz, 2H), 7.76 (d, *J* = 2.1 Hz, 1H), 7.70 (t, *J* = 7.4 Hz, 1H), 7.59 (t, *J* = 7.7 Hz, 2H), 7.56 (dd, *J* = 8.5, 2.0 Hz, 1H). **^{13}C NMR** (126 MHz, DMSO-d_6) δ 189.4, 137.7, 137.6, 136.1, 135.6, 133.9, 131.8, 130.3, 129.9, 129.3, 129.1, 128.4, 125.8. **HRMS** (ESI) m/z: $[M+H]^+$ calculated for $C_{15}H_{11}Cl_2O$: 277.0187; found: 277.0190.

(E)-1-(2,4-Dibromophenyl)-3-phenylprop-2-en-1-one (3ac)

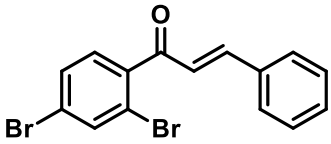

80% yield; yellowish brown solid; m.p. 135-136°C; **^{1}H NMR** (500 MHz, DMSO-d_6) δ 8.28 (s, 1H), 8.18 (d, *J* = 8.5 Hz, 2H), 8.04 (d, *J* = 15.6 Hz, 1H), 7.97 (d, *J* = 15.6 Hz, 1H), 7.76 (s, 1H), 7.72 – 7.68 (m, 1H), 7.59 (t, *J* = 7.7 Hz, 2H), 7.56 (d, *J* = 8.5 Hz, 1H). **^{13}C NMR** (126 MHz, DMSO-d_6) δ 189.6, 137.8, 137.6, 136.1, 135.7, 133.9, 131.8, 130.3, 129.9, 129.4, 129.1, 128.4, 125.8. **HRMS** (ESI) m/z: $[M+H]^+$ calculated for $C_{15}H_{11}Br_2O$: 364.9177; found: 364.9175.

(E)-1-(Naphthalen-1-yl)-3-phenylprop-2-en-1-one (3ad)

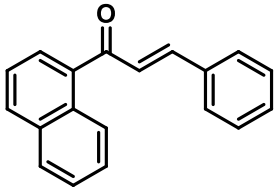

71% yield; light yellow solid; m.p. 188-190°C; **^{1}H NMR** (500 MHz, DMSO-d_6) δ 8.70 (s, 2H), 8.26 (d, *J* = 8.6 Hz, 4H), 8.00 (d, *J* = 4.6 Hz, 4H), 7.92 (dd, *J* = 6.6, 3.1 Hz, 4H), 7.77 (d, *J* = 15.6 Hz, 2H), 7.57 (d, *J* = 7.3 Hz, 4H), 7.48 (d, *J* = 5.1 Hz, 5H), 7.41 (d, *J* = 8.5 Hz, 4H). **^{13}C NMR** (126 MHz, DMSO-d_6) δ 188.5, 156.2, 144.2, 136.2, 135.4, 132.5, 131.1, 130.5, 129.5, 129.4, 122.5, 121.7. **HRMS** (ESI) m/z: $[M+H]^+$ calculated for $C_{19}H_{15}O$: 259.1123; found: 259.1126.

(E)-3-Phenyl-1-(thiophen-2-yl)prop-2-en-1-one (3ae)

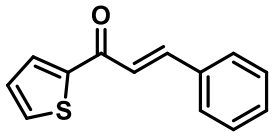

70% yield; grey solid; m.p. 99-100°C; **^{1}H NMR** (500 MHz, $CDCl_3$) δ 7.91 – 7.86 (m, 2H), 7.71 (dd, *J* = 4.9, 1.0 Hz, 1H), 7.68 (dd, *J* = 6.5, 3.1 Hz, 2H), 7.45 (dd, *J* = 8.9, 6.6 Hz, 4H), 7.23 – 7.21 (m, 1H). **^{13}C NMR** (126 MHz, $CDCl_3$) δ 182.1, 145.5, 144.1, 134.7, 133.9, 131.8, 130.6, 128.9, 128.5, 128.2, 121.7. **HRMS** (ESI) m/z: $[M+H]^+$ calculated for $C_{13}H_{11}SO$: 215.0531; found: 215.0530.

(E)-3-Phenyl-1-(pyridin-2-yl)prop-2-en-1-one (3af)

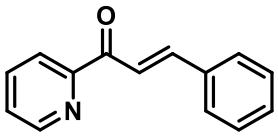

65% yield; brown red liquid; **^{1}H NMR** (500 MHz, $CDCl_3$) δ 7.90 (d, *J* = 8.4 Hz, 2H), 7.79 (d, *J* = 15.6 Hz, 1H), 7.67 (d, *J* = 8.3 Hz, 2H), 7.35 (d, *J* = 15.6 Hz, 1H), 7.26 (dd, *J* = 8.3, 1.9 Hz, 3H), 7.18 (d, *J* = 1.8 Hz, 1H), 6.93 (d, *J* = 8.3 Hz, 1H). **^{13}C NMR** (126 MHz, $CDCl_3$) δ 189.5, 151.7, 149.3, 145.6, 131.9, 129.9, 127.7, 123.3, 119.5, 111.2, 110.2. **HRMS** (ESI) m/z: $[M+H]^+$ calculated for $C_{14}H_{12}NO$ 210.2555; found: 210.2553.

(E)-3-(3,4-Dimethoxyphenyl)-1-(4-methoxyphenyl)prop-2-en-1-one (3ag)

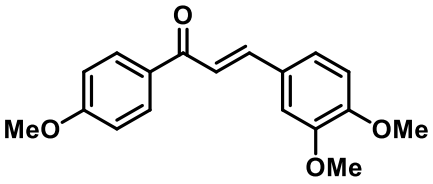

75% yield; yellowish brown solid; m.p. 101-103°C; **^{1}H NMR** (500 MHz, $CDCl_3$) δ 8.03 (d, *J* = 8.9 Hz, 2H), 7.74 (d, *J* = 15.5 Hz, 1H), 7.41 (d, *J* = 15.4 Hz, 1H), 7.16 (s, 1H), 6.96 (d, *J* = 8.9 Hz, 2H), 6.89 (dd, *J* = 15.6, 8.6 Hz, 2H), 3.94 (d, *J* = 4.6 Hz, 3H), 3.91 (d, *J* = 6.7 Hz, 3H), 3.85 (d, *J* = 9.9 Hz, 3H). **^{13}C NMR** (126 MHz, $CDCl_3$) δ 190.9, 163.3, 151.3, 149.2, 144.1, 130.7, 130.6, 128.1, 123.0, 119.7, 113.8, 111.1, 110.4, 56.1, 55.9, 55.4. **HRMS** (ESI) m/z: $[M+H]^+$ calculated for $C_{18}H_{19}O_4$: 299.1283; found: 299.1280.

4.8 Spectral data of few compounds

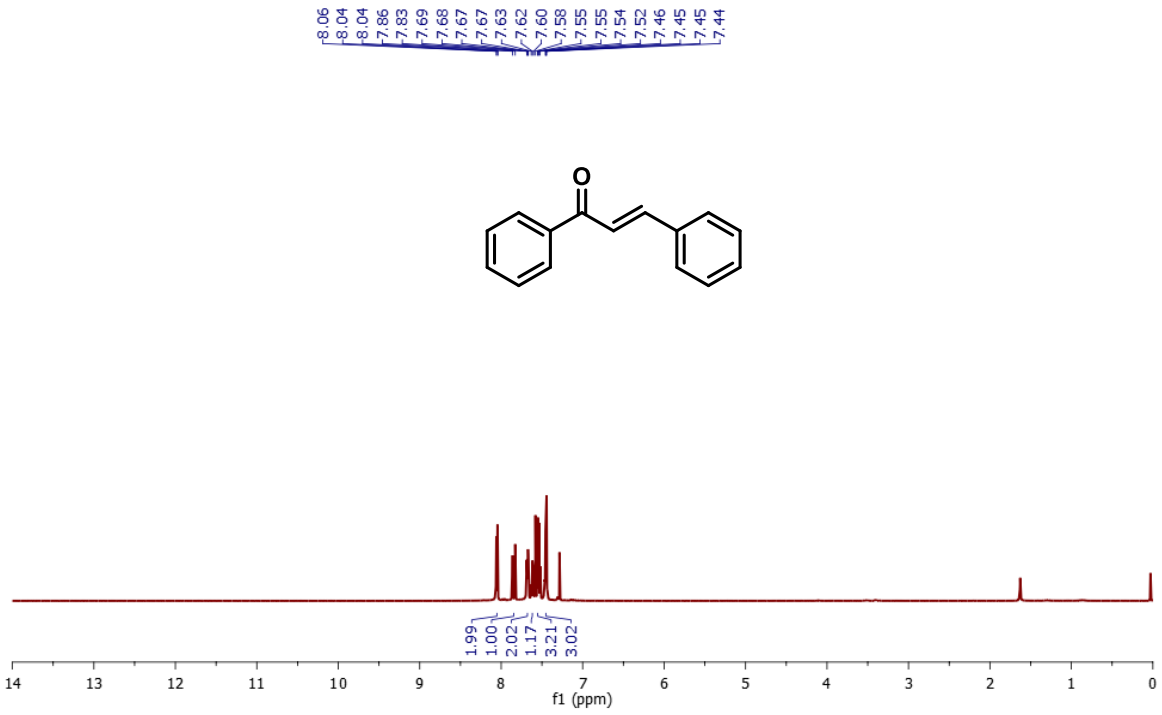

Figure 4.6 ^{1}H-NMR spectrum of **3a** (500 MHz, $CDCl_3$)

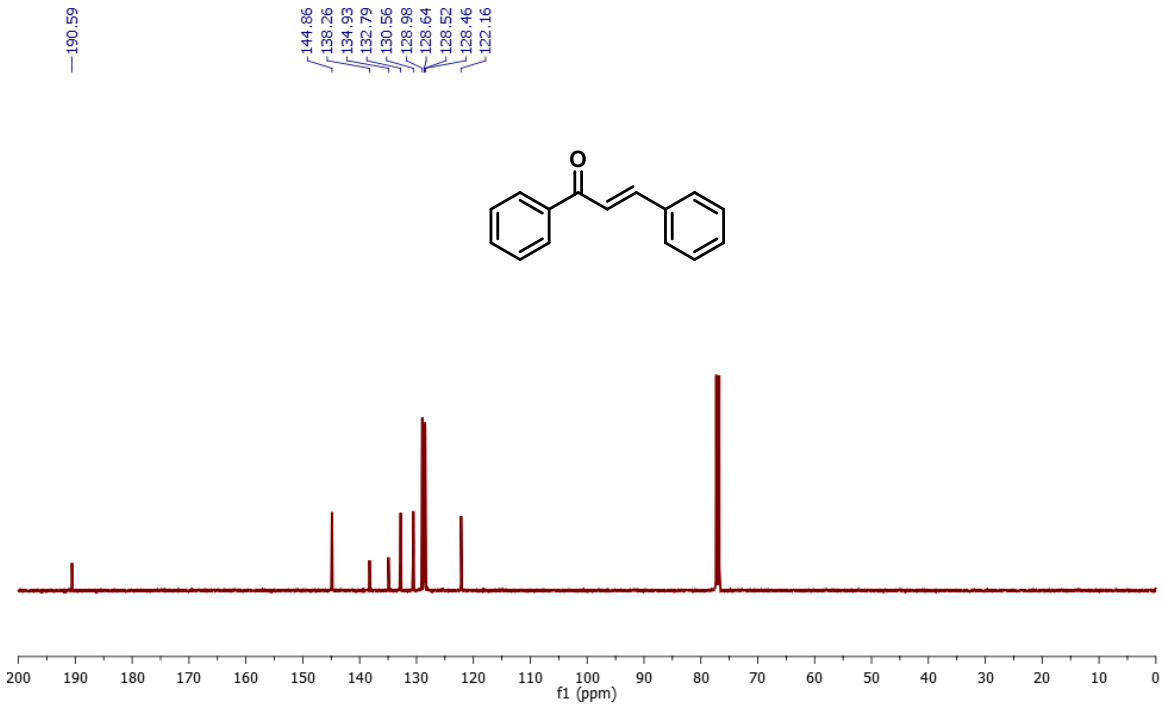

Figure 4.7 ^{13}C-NMR spectrum of **3a** (126 MHz, $CDCl_3$)

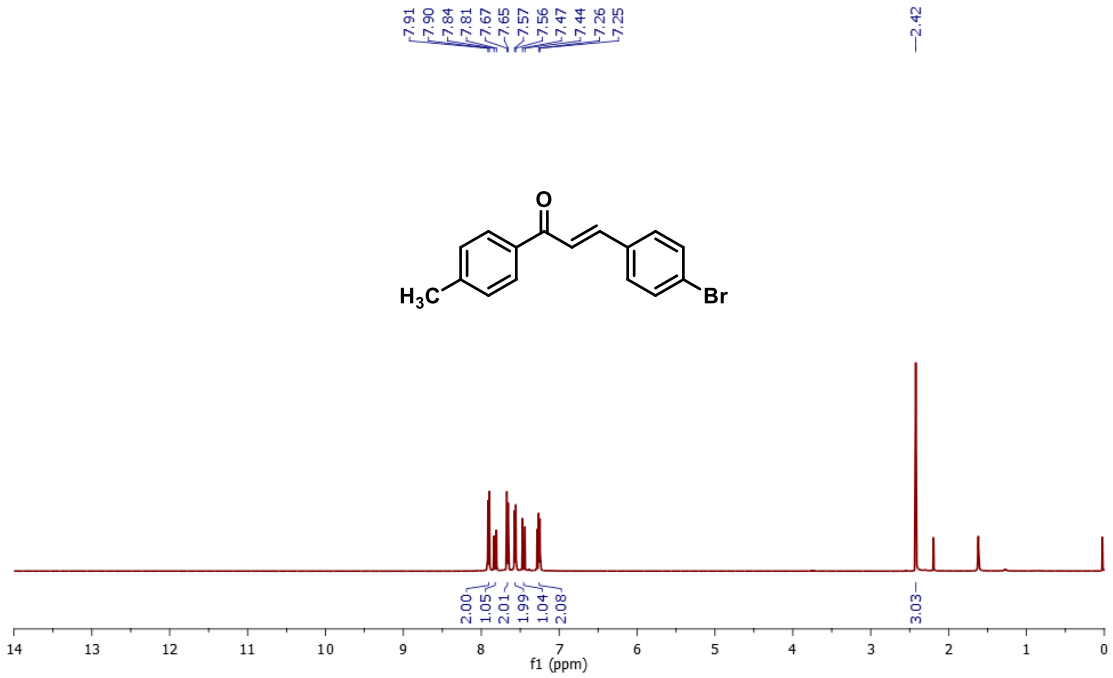

Figure 4.8 ^{1}H-NMR spectrum of **3r** (500 MHz, $CDCl_3$)

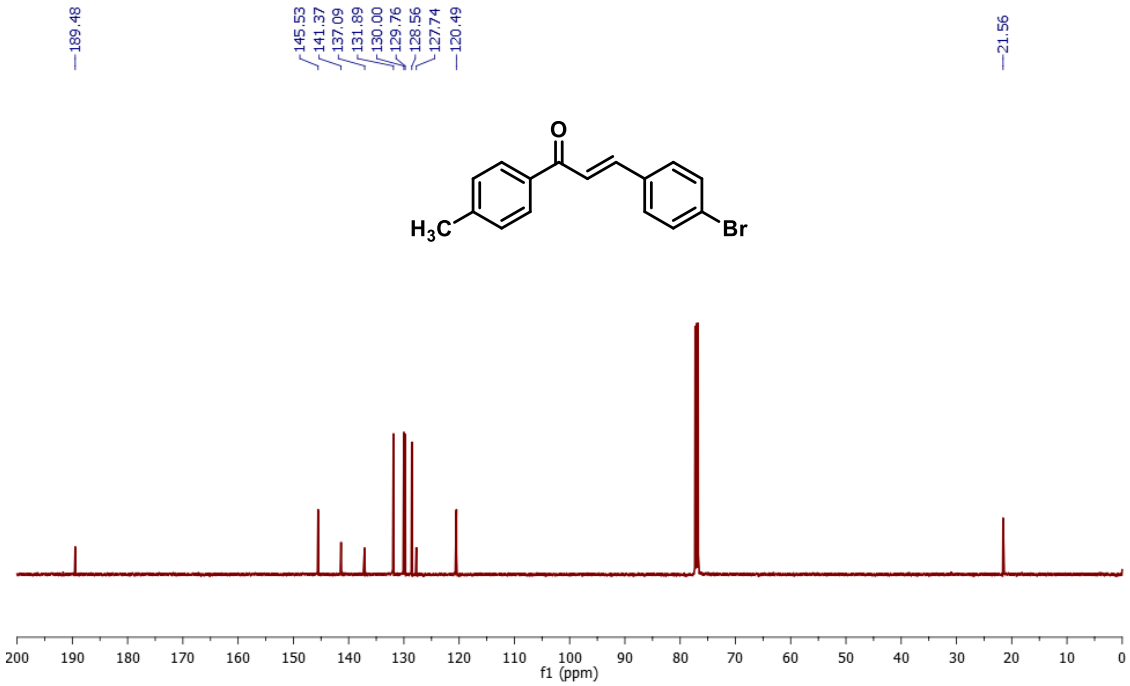

Figure 4.9 ^{13}C-NMR spectrum of **3r** (126 MHz, $CDCl_3$)

4.9 HRMS Data

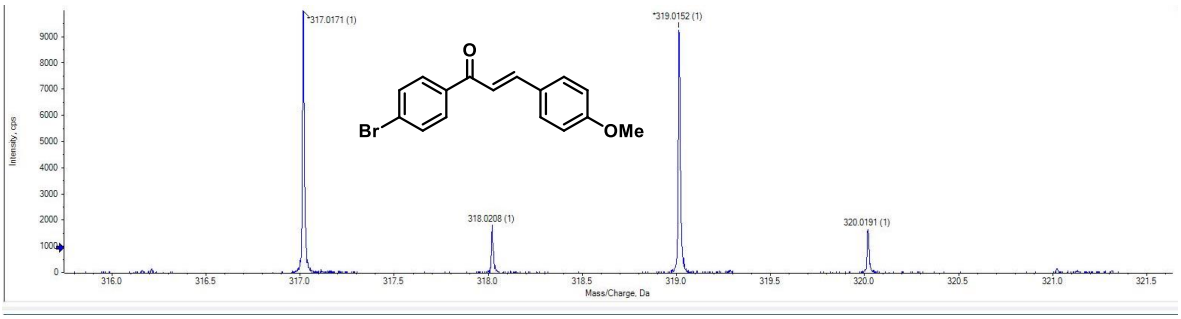

Figure 4.10 HRMS of compound **3j**

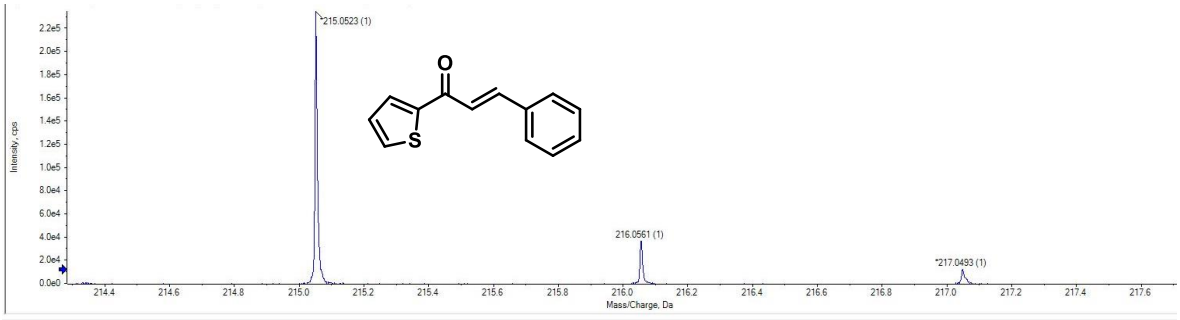

Figure 4.11 HRMS of compound **3ae**

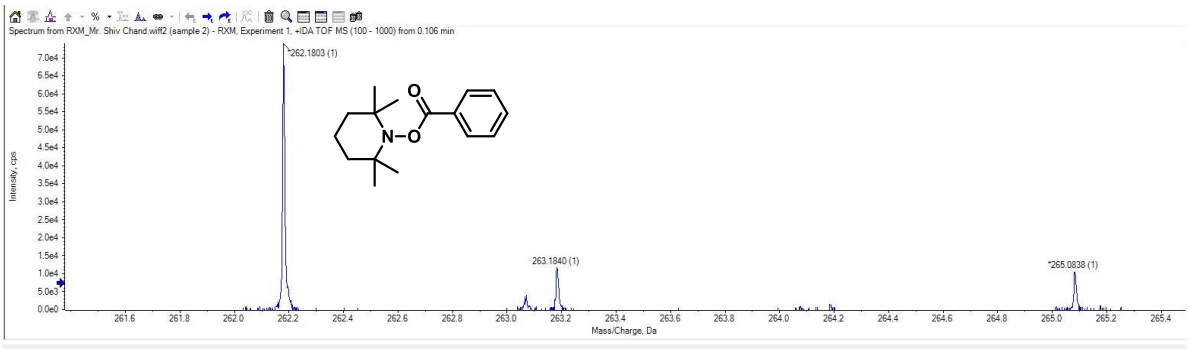

Figure 4.12 HRMS of adduct **4a**

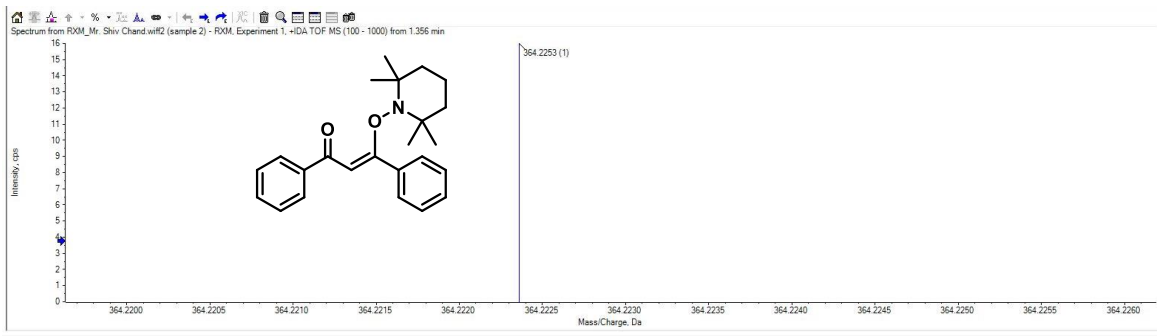

Figure 4.13 HRMS of adduct **5a**

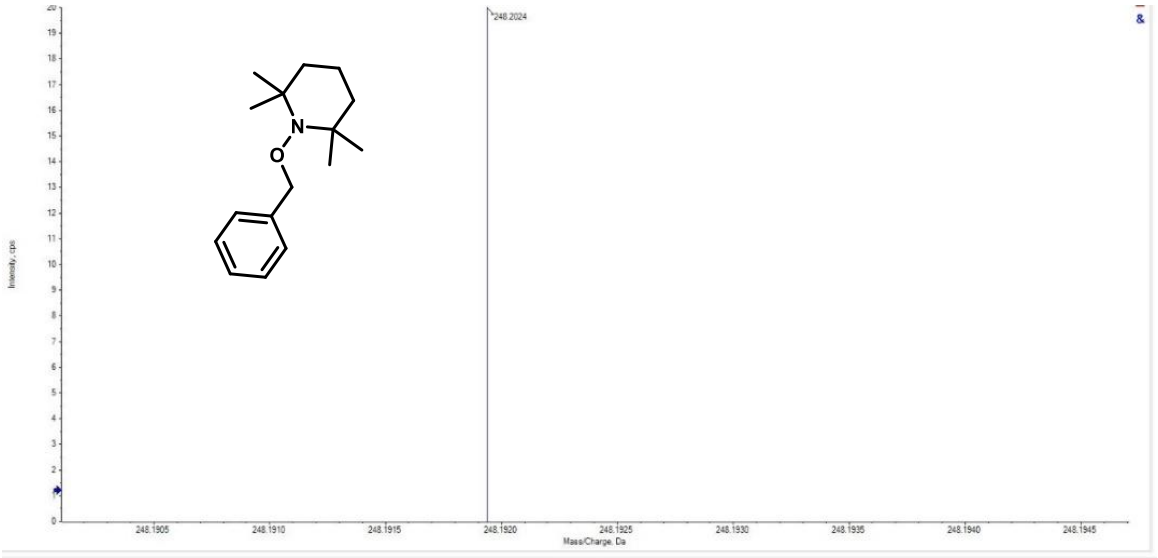

Figure 4.14 HRMS of adduct **6a**

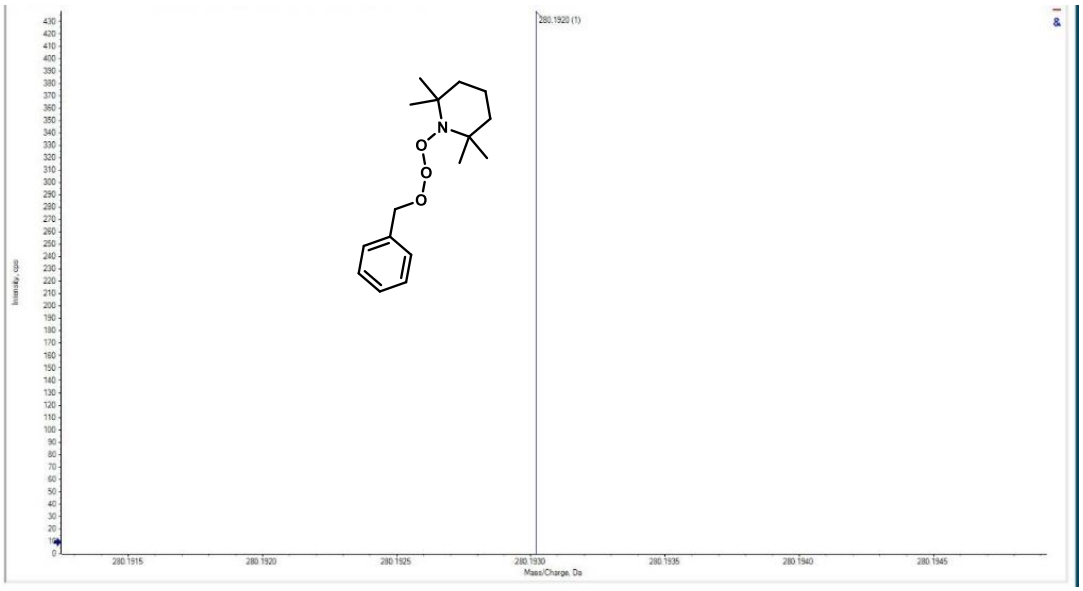

Figure 4.15 HRMS of adduct **7a**

4.10 References

[1] B. Zhao, Y. Wu, Y. Yuan, Z. Shi, Copper-catalysed Csp 3–Csp cross-couplings between cyclobutanone oxime esters and terminal alkynes induced by visible light, Chemical Communications, 56 (2020) 4676-4679.
[2] C. Zhou, T. Lei, X.-Z. Wei, C. Ye, Z. Liu, B. Chen, C.-H. Tung, L.-Z. Wu, Metal-free, redox-neutral, site-selective access to heteroarylamine via direct radical–radical cross-coupling powered by visible light photocatalysis, Journal of the American Chemical Society, 142 (2020) 16805-16813.
[3] J. Zeng, J.-P. Wan, Y. Liu, Photocatalytic C–H Thiocyanation of NH_2-Enaminones and the Tunable Synthetic Routes to 2-Aminothiazoles and 2-Thiazolinones, The Journal of Organic Chemistry, 87 (2022) 13195-13203.
[4] C.-S. Wang, P.H. Dixneuf, J.-F.o. Soulé, Photoredox catalysis for building C–C bonds from C (sp2)–H bonds, Chemical reviews, 118 (2018) 7532-7585.
[5] Q. Liu, L.-Z. Wu, Recent advances in visible-light-driven organic reactions, National Science Review, 4 (2017) 359-380.
[6] S. Roy, S. Panja, S.R. Sahoo, S. Chatterjee, D. Maiti, Enroute sustainability: metal free C–H bond functionalisation, Chemical Society Reviews, 52 (2023) 2391-2479.
[7] W. Liu, Z. Chen, L. Li, H. Wang, C.J. Li, Transition-Metal-Free Coupling of Alkynes with α-Bromo Carbonyl Compounds: An Efficient Approach towards β, γ-Alkynoates and Allenoates, Chemistry–A European Journal, 22 (2016) 5888-5893.
[8] E.-i. Negishi, L. Anastasia, Palladium-catalyzed alkynylation, Chemical reviews, 103 (2003) 1979-2018.
[9] Z.-Z. Zhang, B. Liu, C.-Y. Wang, B.-F. Shi, Cobalt (III)-catalyzed C2-selective C–H alkynylation of indoles, Organic letters, 17 (2015) 4094-4097.
[10] S. Patai, Z. Rappoport, The Chemistry of Triple-Bonded Functional Groups, Supplement C2, Volume 2, Wiley-Blackwell, 1994.
[11] A. Ghosh, K.F. Johnson, K.L. Vickerman, J.A. Walker, L.M. Stanley, Recent advances in transition metal-catalysed hydroacylation of alkenes and alkynes, Organic Chemistry Frontiers, 3 (2016) 639-644.
[12] M.C. Willis, Transition metal catalyzed alkene and alkyne hydroacylation, Chemical reviews, 110 (2010) 725-748.
[13] D.C. Fabry, M. Rueping, Merging visible light photoredox catalysis with metal catalyzed C–H activations: on the role of oxygen and superoxide ions as oxidants, Accounts of chemical research, 49 (2016) 1969-1979.
[14] V. Murugesan, A. Muralidharan, G.V. Anantharaj, T. Chinnusamy, R. Rasappan, Photoredox–Ni Dual Catalysis: Chelation-Free Hydroacylation of Terminal Alkynes, Organic Letters, 24 (2022) 8435-8440.
[15] T. Yatabe, N. Mizuno, K. Yamaguchi, Transition-Metal-Free Catalytic Formal Hydroacylation of Terminal Alkynes, ACS Catalysis, 8 (2018) 11564-11569.
[16] T.S. Ibrahim, A.H. Moustafa, A.J. Almalki, R.M. Allam, A. Althagafi, S. Md, M.F. Mohamed, Novel chalcone/aryl carboximidamide hybrids as potent anti-inflammatory via inhibition of prostaglandin E2 and inducible NO synthase activities: design, synthesis,

molecular docking studies and ADMET prediction, Journal of enzyme inhibition and medicinal chemistry, 36 (2021) 1067-1078.
[17] H. ur Rashid, Y. Xu, N. Ahmad, Y. Muhammad, L. Wang, Promising anti-inflammatory effects of chalcones via inhibition of cyclooxygenase, prostaglandin E2, inducible NO synthase and nuclear factor κb activities, Bioorganic Chemistry, 87 (2019) 335-365.
[18] J. Higgs, C. Wasowski, A. Marcos, M. Jukič, C.H. Pavan, S. Gobec, F. de Tezanos Pinto, N. Colettis, M. Marder, Chalcone derivatives: synthesis, in vitro and in vivo evaluation of their anti-anxiety, anti-depression and analgesic effects, Heliyon, 5 (2019) e01376.
[19] B. Lakshminarayanan, N. Kannappan, T. Subburaju, Synthesis and biological evaluation of novel chalcones with methanesulfonyl end as potent analgesic and anti-inflammatory agents, Int. J. Pharmaceutical Res. Biosci, 11 (2020) 4974-4981.
[20] A.T. Bale, U. Salar, K.M. Khan, S. Chigurupati, T. Fasina, F. Ali, M. Ali, S.S. Nanda, M. Taha, S. Perveen, Chalcones and Bis-Chalcones Analogs as DPPH and ABTS Radical Scavengers, Letters in Drug Design & Discovery, 18 (2021) 249-257.
[21] M. Čižmáriková, P. Takáč, G. Spengler, A. Kincses, M. Nové, M. Vilková, J. Mojžiš, New chalcone derivative inhibits ABCB1 in multidrug resistant T-cell lymphoma and colon adenocarcinoma cells, Anticancer Research, 39 (2019) 6499-6505.
[22] N. Fakhrudin, K.K. Pertiwi, M.I. Takubessi, E.F. Susiani, A. Nurrochmad, S. Widyarini, A. Sudarmanto, A.A. Nugroho, S. Wahyuono, A geranylated chalcone with antiplatelet activity from the leaves of breadfruit (Artocarpus altilis), Pharmacia, 67 (2020) 173-180.
[23] S. Welday Kahssay, G.S. Hailu, K. Taye Desta, Design, Synthesis, Characterization and in vivo Antidiabetic Activity Evaluation of Some Chalcone Derivatives, Drug Design, Development and Therapy, (2021) 3119-3129.
[24] M.R. Reddy, I.S. Aidhen, U.A. Reddy, G.B. Reddy, K. Ingle, S. Mukhopadhyay, Synthesis of 4-C-β-D-Glucosylated Isoliquiritigenin and Analogues for Aldose Reductase Inhibition Studies, European Journal of Organic Chemistry, 2019 (2019) 3937-3948.
[25] G. Aljohani, A. Al-Sheikh Ali, S.Y. Alraqa, S. Itri Amran, N. Basar, Synthesis, molecular docking and biochemical analysis of aminoalkylated naphthalene-based chalcones as acetylcholinesterase inhibitors, Journal of Taibah University for Science, 15 (2021) 781-797.
[26] P. Bhoj, N. Togre, S. Bahekar, K. Goswami, H. Chandak, M. Patil, Immunomodulatory activity of sulfonamide Chalcone compounds in mice infected with filarial parasite, Brugia malayi, Indian Journal of Clinical Biochemistry, 34 (2019) 225-229.
[27] T.H. Bui, N.T. Nguyen, P.H. Dang, H.X. Nguyen, M.T.T. Nguyen, Design and synthesis of chalcone derivatives as potential non-purine xanthine oxidase inhibitors, SpringerPlus, 5 (2016) 1-8.
[28] S. Saini, K. Kumar, P. Saini, D.K. Mahawar, K.S. Rathore, S. Kumar, A. Dandia, V. Parewa, Sustainable synthesis of biomass-derived carbon quantum dots and their catalytic

application for the assessment of α, β-unsaturated compounds, RSC advances, 12 (2022) 32619-32629.
[29] S. Verma, D. Twilley, T. Esmear, C.B. Oosthuizen, A.-M. Reid, M. Nel, N. Lall, Anti-SARS-CoV natural products with the potential to inhibit SARS-CoV-2 (COVID-19), Frontiers in Pharmacology, 11 (2020) 561334.
[30] H.A. Elshabrawy, SARS-CoV-2: An update on potential antivirals in light of SARS-CoV antiviral drug discoveries, Vaccines, 8 (2020) 335.
[31] B. Bhat, Dhar? KL; Puri, SC; Saxena, AK; Shanmugavel, M.; Qazi, GN, Bioorg. Med, Chem, Lett, 15 (2005) 3177-3180.
[32] E. Saraci, M. Andreoli, E. Casali, M. Verzini, M. Argese, R. Fanelli, G. Zanoni, Solvent-free synthesis of chalcones using Mg (HSO4) 2, RSC Sustainability, 1 (2023) 504-510.
[33] S. Tripathi, R. Kapoor, L.D.S. Yadav, Visible Light Activated Radical Denitrative Benzoylation of β-Nitrostyrenes: A Photocatalytic Approach to Chalcones, Advanced Synthesis & Catalysis, 360 (2018) 1407-1413.
[34] K. Tanemura, Large acceleration under highly concentrated conditions: Synthesis of chalcones using a small amount of DMF or [emim] N (CN) 2, Results in Chemistry, 4 (2022) 100316.
[35] C. Zhuang, W. Zhang, C. Sheng, W. Zhang, C. Xing, Z. Miao, Chalcone: a privileged structure in medicinal chemistry, Chemical reviews, 117 (2017) 7762-7810.
[36] J.H. Rhlee, S. Maiti, J.W. Lee, H.S. Lee, I.A. Bakhtiyorzoda, S. Lee, J. Park, S.J. Kang, Y.S. Kim, J.K. Seo, Synthesis of α, β-unsaturated ketones through nickel-catalysed aldehyde-free hydroacylation of alkynes, Communications Chemistry, 5 (2022) 13.
[37] A. Mondal, R. Hazra, J. Grover, M. Raghu, S. Ramasastry, Organophosphine-catalyzed intramolecular hydroacylation of activated alkynes, ACS Catalysis, 8 (2018) 2748-2753.
[38] J.F. Hooper, S. Seo, F.R. Truscott, J.D. Neuhaus, M.C. Willis, α-Amino aldehydes as readily available chiral aldehydes for Rh-catalyzed alkyne hydroacylation, Journal of the American Chemical Society, 138 (2016) 1630-1634.
[39] Q.-A. Chen, F.A. Cruz, V.M. Dong, Alkyne hydroacylation: switching regioselectivity by tandem ruthenium catalysis, Journal of the American Chemical Society, 137 (2015) 3157-3160.
[40] J. Wu, W.-X. Gao, X.-B. Huang, Y.-B. Zhou, M.-C. Liu, H.-Y. Wu, Cobalt-catalyzed selective hydroacylation of alkynes, Organic Chemistry Frontiers, 8 (2021) 6048-6052.
[41] W. Shi, C. Yang, L. Guo, W. Xia, Photo-induced decarboxylative hydroacylation of α-oxocarboxylic acids with terminal alkynes by radical addition–translocation–cyclization in water, Organic Chemistry Frontiers, 9 (2022) 6513-6519.
[42] B. Sun, Y. Wang, J. Wang, M. Chen, Z. Zhong, J. Wang, C. Jin, Photoredox-Catalyzed Redox-Neutral Decarboxylative C–H Acylations of Coumarins with α-Keto Acid, Organic Letters, 25 (2023) 2466-2470.
[43] Y. Zhang, W. Schilling, S. Das, Metal-Free Photocatalysts for C− H Bond Oxygenation Reactions with Oxygen as the Oxidant, ChemSusChem, 12 (2019) 2898-2910.

[44] S.G. Amos, M. Garreau, L. Buzzetti, J. Waser, Photocatalysis with organic dyes: Facile access to reactive intermediates for synthesis, Beilstein journal of organic chemistry, 16 (2020) 1163-1187.
[45] M. Forchetta, F. Valentini, V. Conte, P. Galloni, F. Sabuzi, Photocatalyzed Oxygenation Reactions with Organic Dyes: State of the Art and Future Perspectives, Catalysts, 13 (2023) 220.
[46] H.K. Singh, A. Kamal, S. Kumari, S.K. Maury, A.K. Kushwaha, V. Srivastava, S. Singh, Visible-Light-Promoted Synthesis of Fusesd Imidazoheterocycle by Eosin Y under Metal-Free and Solvent-Free Conditions, ChemistrySelect, 6 (2021) 13982-13991.
[47] S.K. Maury, S. Kumari, A. Kamal, H. kumar Singh, D. Kumar, Visible Light Initiated Oxidative Coupling of Indole and Active Methylene Compounds Using Eosin Y as a Photocatalyst, Synthesis, (2022).
[48] S.K. Maury, A.K. Kushwaha, A. Kamal, H.K. Singh, S. Singh, Visible light triggered synthesis of spiro [indoline-3, 4′-quinoline] via oxidative coupling of indole with enaminone and malononitrile, Journal of Molecular Structure, 1274 (2023) 134452.
[49] A. Kamal, H.K. Singh, D. Kumar, S.K. Maury, S. Kumari, V. Srivastava, S. Singh, Visible Light-Induced Cu-Catalyzed Synthesis of Schiff's Base of 2-Amino Benzonitrile Derivatives and Acetophenones, ChemistrySelect, 6 (2021) 52-58.
[50] A.K. Kushwaha, S.K. Maury, A. Kamal, H.K. Singh, S. Pandey, S. Singh, Visible-light-absorbing C–N cross-coupling for the synthesis of hydrazones involving C (sp 2)–H/C (sp 3)–H functionalization, Chemical Communications, 59 (2023) 4075-4078.
[51] A. Kamal, H.K. Singh, S.K. Maury, A.K. Kushwaha, V. Srivastava, S. Singh, Photo-Triggered Synthesis of Sulfonamides in a Sustainable Solvent via Electron Donor-Acceptor Complex, Asian Journal of Organic Chemistry, 12 (2023) e202200632.
[52] H. kumar Singh, A. Kamal, S.K. Maury, A.K. Kushwaha, V. Srivastava, S. Singh, A Green Synthesis of N-heterocyclic Pyrimido [4, 5-b] Quinolines and Pyrido [2, 3-d] Pyrimidines via mechanochemical approach, Organic & Biomolecular Chemistry, (2023).
[53] S.P. Singh, V. Srivastava, P.K. Singh, P.P. Singh, Visible-light induced eosin Y catalysed C (sp2)-H alkylation of carbonyl substrates via direct HAT, Tetrahedron, (2023) 133245.
[54] M. Uygur, J.H. Kuhlmann, M.C. Pérez-Aguilar, D.G. Piekarski, O.G. Mancheño, Metal-and additive-free C–H oxygenation of alkylarenes by visible-light photoredox catalysis, Green Chemistry, 23 (2021) 3392-3399.
[55] J. Yan, H. Tang, E.J.R. Kuek, X. Shi, C. Liu, M. Zhang, J.L. Piper, S. Duan, J. Wu, Divergent functionalization of aldehydes photocatalyzed by neutral eosin Y with sulfone reagents, Nature Communications, 12 (2021) 7214.